ABSTRACT

An aerodynamic analysis has been performed in order to relate the lift, drag forces for different airfoils. Take-off and Climb mainly burn the most fuel for a given time or distance in aircraft. In terms of time, it is moderately more fuel, typically about 30-40% more. Variations in design can subsequently affect its performance to upward force. For this reason, a trade-off study has been analyzed for airfoil profiles of numerous designs. NACA 2412 has been selected for the optimized design. The results have been perused and conclusions about a number of different designs made with a subsequent selection of airfoil designs which have been depicted for a high L/D ratio. During the design process, symmetric airfoils and cambered airfoils have been analyzed in several features with respect to low wind speed. In order to produce an efficacious design, the range of changes of the angle of attack with a small incremental on various parameters were adjusted to different airfoils. Test data of two dimensional NACA four digit airfoils and modifications were appraised. The response variables such as Lift-coefficient, drag-coefficient and design variables such as angle of attack, maximum camber, thickness were analyzed to confirm the aerodynamic measurement system and to produce better Lift over Drag ratio. This analysis includes the aerodynamic performance which meant obtaining lift and reducing drag coefficients through scatter plots and curves as a function of the angle of attack experimentally for the situation where the performance of the aerial vehicle is maximized and the fuel consumption is minimized in the most efficient angle of attack condition. All the figures were drawn using Python software for data visualization.

.

Table of Contents

List of Tables

NOMENCLATURE

C_d	Coefficient of Drag
C_l	Coefficient of Lift
Cn	Normal Force Coefficient
Cp	Coefficient of Pressure
r	Direction along radius of curvature
Ctip	Tip Chord
D	Drag Force
L	Lift Force
L/D	Lift to Drag Ratio
p	Pressure
P∞	Free Stream Pressure
Pl	Local Static Surface Pressure
$q\infty$	Dynamic Pressure
r0	Radius of Curvature at Airfoil's Leading Edge
Re	Reynolds Number
tmax	Maximum Thickness of Airfoils.
V∞	Free Stream Velocity of Air
v	Velocity of Air
R	Radius of curvature
maxcamberpostion	Distance of Maximum Camber
maxcamber	Maximum Camber
α , AOA	Angle of Attack
CLmax AOA, α_{lMAX}	Stalling Angle of Attack
L/D_{max} aoa	Effective Angle of Attack
$1/2\ \rho U\infty^2$	Free Stream Dynamic Pressure

Chapter 1

Introduction

An airfoil is the cross-sectional geometry of any lifting or propelling device (i.e. wings, blades, etc.). When a body with an airfoil-shaped device or of a shape of an airfoil moves through fluid flow, lift and drag forces are generated which are exerted on the airfoil. The force component that works normally to the direction of motion is called lift force and the force component that works parallel to the motion is called drag force. [1]

Perception from bird wings:

The earliest but not frivolous project on the development of airfoil sections began in the late 1800s. In the 1880s, Lilienthal discovered the specific shape from the bird's wings, which inspired the airplane invention by Wright brothers.[6]

Albeit it was clear that flat plates would produce lift when set at a distinct angle of incidence, some were dubious that shapes with curvature, that more closely resembled bird wings would produce more lift or do so more with efficacy. H.F. Phillips patented a series of airfoil shapes in 1884 after testing them in one of the earliest wind tunnels in which "artificial currents of air (were) produced from induction by a steam jet in a wooden trunk or conduit." Octave Chanute writes in 1893, "it seems very desirable that further scientific experiments were been able to make on concave surfaces of varying shapes, for it is plausible that the difference between success and failure of a proposed flying machine will depend on the sustaining effect between a plane surface and one properly curved to get a maximum amount of 'lift'." At nearly the same time Otto Lilienthal had some akin ideas. After measuring deliberately, the shapes of bird wings, he experimented with the airfoils (reproduced from his 1894 book, 'Bird Flight as the Basis of Aviation) on a 7m diameter "whirling machine". Lilienthal believed that the key to uncurbed flight was wing curvature or camber. He also experimented with different nose radii and thickness distributions.[1,4]

Airfoils discovered by the Wright Brothers closely resembled Lilienthal's sections: thin and highly cambered. This was quite plausible because early tests of airfoil sections were done at extremely low Reynolds number, where such sections behave much better than thicker ones. The erroneous notion, that efficient airfoils had to be thin and highly cambered, was one cause behind that some of the first airplanes were biplanes.[2]

A wide range of airfoils was developed, based primarily on trial and error. Some of the more successful sections such as the Clark Y and Gottingen 398 were used as the basis for a family of sections tested by the NACA in the early 1920s.[5]

A flat sheet makes a perfectly serviceable wing. That flat surfaces in the wind could produce the sideways force that we now call lift was a very ancient observation. Two early applications of it, the windmill and the fore-aft rigged sail date back at least 800 years. It was also perfectly evident to any thinking person that what kept birds and bats aloft was the large flat surfaces attached to their arms.

Neither the feathers of birds nor the fabric of sails and windmill blades had any thickness to speak of, and so the earliest lifting surfaces were just that surfaces.[5]

Thin surfaces restrained by a supporting structure naturally swelled out under air pressure, assuming what we now call a "cambered" -- that is, arched shape. The fact that camber was beneficial seems first to have been commended -- at least in writing -- by an English civil engineer of the 18th century, John Smeaton, who noted that curving the surfaces of their blades improved the performance of windmills.[3]

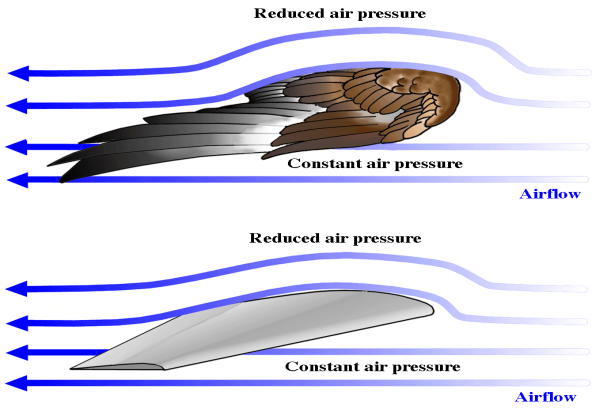

Figure 1.1: Reconciliation of Bird wing and Aircraft wing [4]

Wright brothers' systematic wind tunnel:

Arriving at the beginning of the 20th century, we see the Wrights conducting systematic wind tunnel experiments to ascertain not only the best amount of camber to utilize but also the best fore-and-aft distribution of curvature.[4] The Brazilian Santos-Dumont, whose 1906 Paris flights in his huge 14-bis ("Number 14 encore") are thought by some to have been the first real powered flights as his airplane twisted and rose under its power (the Wrights employed a catapult and rail to obtain airborne in 1903), used very scant camber, perhaps because he knew that it created an aircraft want to dive. On the other hand, the wings of the Bleriot 11 that made the first aerial crossing of the English Channel had a great deal of camber than they required. Airfoils used by the **Wright Brothers** closely resembled Lilienthal's sections: thin and highly cambered. This was quite plausible because early tests of airfoil sections were done at extremely low Reynolds numbers, where such sections behave much better than thicker ones. The erroneous belief that efficient airfoils had to be thin and highly cambered was one reason that some of the first airplanes were biplanes. The use of such sections gradually diminished over the next decade.[5,6].

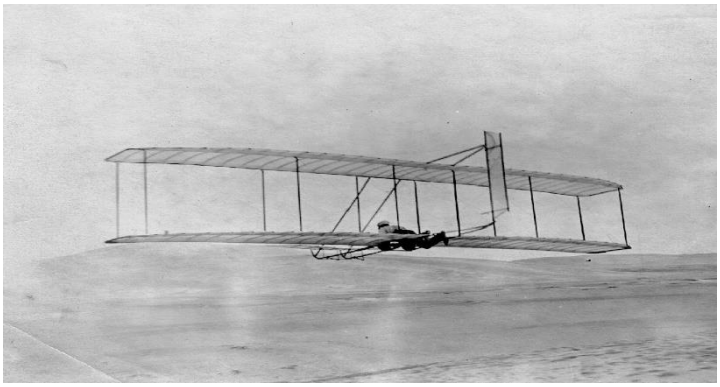

Figure 1.2: First airfoil design of Wright Brothers' in 1902 [6]

Laminar flow airfoil

A wide range of airfoils was developed, based primarily on trial and error. Some of the more successful sections such as the Clark Y and Gottingen 398 were utilized as the basis for a family of sections tested by the NACA in the early 1920s. In 1939, Eastman Jacobs at the NACA in Langley, designed and tested the first laminar flow airfoil sections. These shapes had extremely low drag and the section shown achieved a lift to drag ratio of about 300.[7]. In contradiction to the mathematical methods to calculate the pressure distribution of airfoil, Jacobs proposed the airfoil design which causes the desired pressure distribution. The laminar flow of airfoil was expanded to cause a higher L/D ratio and smaller drag [6]. cause a higher L/D ratio and smaller drag [6].

Later, different types of airfoils for various airplane design and off-design requirements were continuously designed [11]

A modern laminar flow section, used on sailplanes, illustrates that the concept is practical for some applications. It was not thought to be pragmatic for many years after Jacobs demonstrated it in the wind tunnel. Even now, the utility of the concept is not wholly accepted and the "Laminar Flow True-Believers Club" meets each year at the homebuilt aircraft fly-in.[6]

The airfoil used on the Solar Challenger, an aircraft that flew across the English Channel on solar power, was designed with fully a flat upper surface so that solar cells could be easily mounted. In Fig 4.[6]The last two shapes are low-drag sections designed to have laminar flow over 60 to 70 percent of the chord on both the upper and lower surface. One of the reasons why modern airfoils look quite not akin to one another and designers have not settled on the one best airfoil is that the flow conditions and design goals change from one application to the next. At Various Reynolds numbers, efficient airfoil sections can look rather eccentric as suggested by the sketch of a Flat Plate. The thin, highly cambered plate is close to Lilienthal's designs. The NACA0012 was a good section for model airplanes.[9]

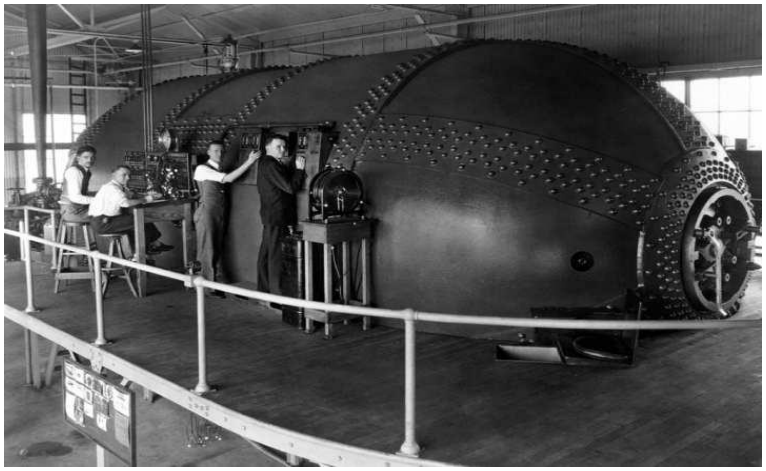

Figure 1.3 The variable density Wind Tunnel[12]

Barefoot Airfoil Clark-Y:

The second milestone was the discovery, due to Prandtl, that thickness -meaning thickness greater than, say, a tenth of the chord length was beneficial. Albeit all the highly technical theoretical work done by NACA, there existed a continuous parallel tradition of what might be called barefoot airfoil design. It grew out of the recognition that the airfoils on real wings, many of which were still covered with fabric during that period, did not contain much resemblance to idealized wind tunnel models. Pragmatically, anything that appeared like an airfoil functioned like an airfoil.[11] The prominent invention of the barefoot school was the Clark Y, a 1922 invention of Colonel Virginia Clark, who arrived at it by the highly unscientific expedient of deforming one of the second world wartime Gottingen airfoils to make the aft 70 percent of its bottom flat[12]. The flat bottom turned out to be a very winsome design. It facilitated construction (especially for modelers, who flocked to the Clark Y as it give them the privilege to make a wing straight by simply pinning it down to a flat surface while the glue is desiccated) and measurement of the angle of attack, and it simplified the curving of propeller blades. Despite its possessing no significant aerodynamic merits, the Clark Y has been used in a wide variety of aircrafts. [17]

During the 1930s the U.S. National Advisory Committee for Aeronautics, or NACA, developed and tested "families" of airfoils. Some of the most successful of these were the NACA four-digit and five-digit series, which consisted of a "basic thickness form", asymmetrical "teardrop" shape-superimposed on a "camber line" from which the profile derived most of its aerodynamic characteristics, such as the amount of lift is produced at an angle of attack of zero, and the strength of the "pitching moment" or diving tendency that camber tended to produce. Many of those sections are still in use today, and NACA's 23000 series, created in 1935, is probably the most prevalent airfoil of history. [17-19]

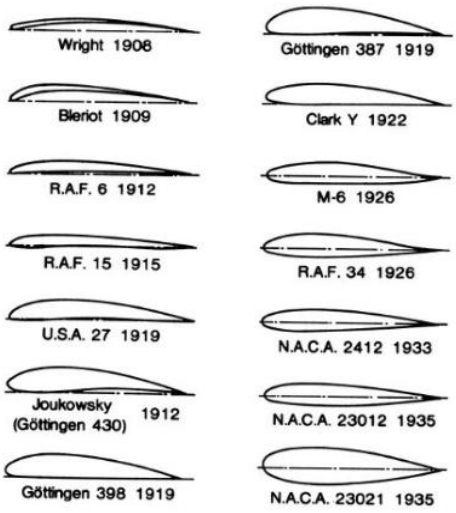

Figure 1.3. Different Airfoil thickness from Icarus to Airplanes. [7]

First prevalent design

The most ubiquitous airfoil of all time was the NACA 23012 combined with high lift, low drag, mild pitching moments, with a bit of laminar flow on its lower surface. It was schemed in 1935 by NACA Langley researcher Eastman Jacobs. He was a leading aerodynamicist who served for NACA's

Langley Memorial Aeronautical Laboratory which was renamed NASA Langley Research Center in 1958. He worked there from the 1920s to 1940.By 1940, airfoil development had passed three milestones[44].The first milestone was the general recognition, not due to any single investigator, that camber aided the production of lift, and that if an airfoil had more than negligible thickness it needed to be rounded in the front and somewhat sharp in the back.[20] The North American NA-35 was a training aircraft designed by North American Aviation. The airfoil is NACA-4416R at root, tapering to NACA-6409R at tip.[24]

It was first test-flown in January 1940 by Vance Breese. Although announced for trade the month after, the project was pushed aside by plant expansions and the development of the P-51 Mustang.[25]

The third milestone was the systematization of profiles -- largely the work of Eastman Jacobs. The primary outcome of Jacobs' travail was the natural laminar flow airfoil. His travail was founded on the perception that the characteristic of the boundary layer -- the thin layer of air, abut to the airfoil surface, that the airplane pulls along with it, is influenced by the pressure distribution. A laminar boundary layer where all the air particles follow paths analogous to the airfoil surface could be maintained along with the countenance of an airfoil, as its upper and lower surfaces grew further apart albeit when the surfaces began to coincide, small turbulent eddies and vortices would appear in the demarcating layer. [21] The drag of a laminar boundary layer is much less than the drag of a tortuous one. All airfoils have some laminar flow, but the new family of laminar airfoils augmented

by the NACA enhanced the laminar boundary layer to as much as sixty percent of the airfoil's length, lessening drag by as much as two-thi

The fourth milestone was a revolution in the reconciliation between mathematics and airfoil design. From the early days, various kinds of mathematical functions had been used to create airfoil shapes. However, these procedures were not based on the physics of fluid. In 1931, another NACA aerodynamicist, Theodore Theodorsen, invented a mathematical process of calculating the pressure distribution on an airfoil. The pressure distribution is of huge primacy as it is the key to the airfoil's drag, lift, and stalling attitude. [23,24]

Theodorsen was a plucky fellow, as his calculated results did not precisely reconcile with wind tunnel measurements, he airily discarded the critically analyzed results as unreliable. Relations between Theodorsen and the experimentalist Eastman Jacobs were pugnacious, and when Jacobs, playing against type, Theodorsen proposed reversing. Theodorsen schemed to gain an airfoil shape that would generate a required pressure distribution, he repudiated the notion as mathematically nonsensical. Jacobs was persistent, however, and he succeeded in forming the process used to design airfoils in digital computers today.[25]

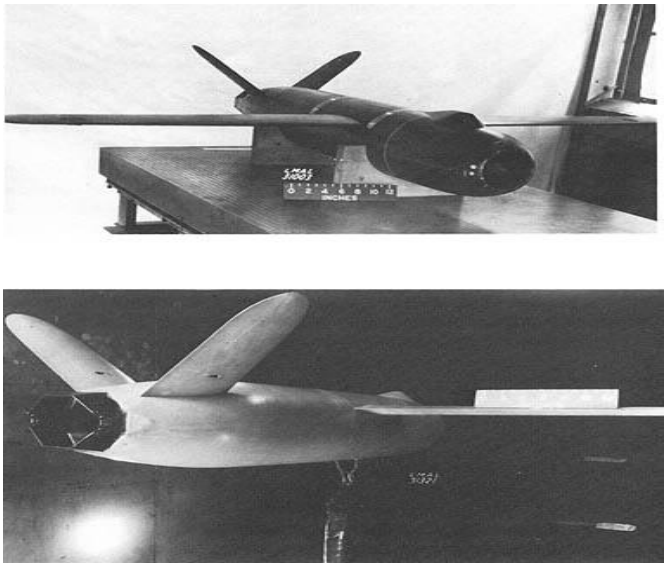

Figure 1. 5: WWII US jet project with butterfly tail developed by eminent Aerodynamicist Eastman Jacobs [24]

The fifth milestone in airfoil evolution comes with the development of foils especially designed for flight below, but close to, the speed of sound. These so-called **supercritical airfoils** have thick noses, flattish tops, and aft camber, all characteristics designed to delay the beginning of shock waves due to local supersonic flow. [23] Since John Anderson alluded in his document “History of Aerodynamics,” the laminar airfoils, first used on the P-51 Mustang, were successful in decreasing drag in the wind tunnel but less efficient in the field because the irregularities of practical metal construction, along with general wear-and-tear and ineluctable bug splatter, would interrupt the temperamental laminar boundary layer. Yet they never refuted to be successful in an unexpected path; laminar-flow sections, with their maximum thickness far aft, turned out to be well-matched for

high-speed aircraft because they were less apt to the early formation of transonic shock waves. Anderson might have included that they had some accomplishments, even in the area and on low-speed airplanes when byzantine wings came into use. A high-performance sailplane with a non-laminar airfoil is implausible today.[29-31]

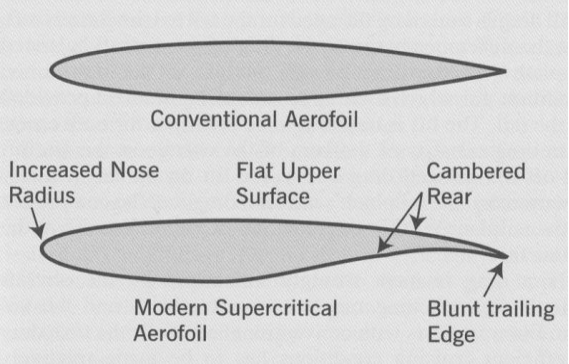

Figure 1.6: Supercritical airfoil with conventional airfoil. [27]

Stepped airfoils development in early 1960

A breakthrough concept in airfoil design was introduced by Richard L.Kline and Floyd F.Fogleman with their stepped airfoils developed in the early 1960s.[23] This opened a new chapter in aerodynamics with the break-through design of high-performance airfoils with extended stalling capabilities and improved lift and drag characteristics. The object of this design was described by The Ultimate Paper Airplane by Richard L.Kline & F.Fogleman and it was to develop an improved airfoil with enhanced lift, drag, and stability characteristics and adaptability over a wide range of speeds, achieved by the generation of vortical flow that alters the flow field resulting in favorable effects. Several other articles published later had also stated that Kline-Fogleman (KF) airfoils were capable of combining the best features of conventional airfoils i.e. better lift with thick ones and higher speeds with thinner ones and further that they worked extremely well for achieving higher lift as well as forward speed. These statements are supported by the world record that Dick Kline still holds for the farthest flying paper plane equipped with stepped airfoils.[24]. In an email that Kline sent to an RC modeling group on issues concerning KF airfoils, he highlighted the advantages of KF airfoils. Most noteworthy ones are the capability of KF airfoils to handle a wide range of speeds; the much greater range for its center of gravity which its case could be moved as much as 40% chord location from the leading edge thus allowing it to carry a heavier load; better air penetration based on the flight experiences of model planes built with KF airfoils; high strength to weight ratio; great stability and control. Some of the earliest citations of airfoils with vortex trapping cavities were made in a paper by Ringleb F.O. (1961).

W.A.Kasper[22] claimed the first successful use of a trapped vortex in a flight experiment in the seventies using a concept so-called as Kasper wing. The Kasper-wing produced vortex shedding as against a steady trapped vortex thus resulting in lift enhancement was verified by the experimental studies undertaken by Kruppa[24] (1977). By the researchers of Saab-Scania (1974) using a wing with a vortex cavity, some promising results were obtained as reported by Kruppa in his paper. In 1994, Demeter G.Fertis[25] scientifically proved the benefits of KF airfoils through experiments and flight testing. He compared the results obtained for the stepped airfoil with those for conventional NACA 23012 airfoil and confirmed that the airfoils developed by Kline and Fogleman were potential designs to obtain better lift characteristics over a broad range of angles of attack, improve or eliminate stall at all possible operational airspeeds, increase lift to drag ratios over a wider range of operational angles of attack and be adaptable for both fixed and rotary-wing aircraft. [31] This set the direction for a new domain in flow control research, which tills then involved focusing on the use of flow control techniques on conventional airfoils. Stephen Withers and Fathi Finaish (1996) conducted aerodynamic studies on stepped airfoils for different configurations defined by the step lengths, depths, and the location of steps on the airfoil chord. Steps on NACA 0012 and 23012 airfoils showed that higher lift coefficients were obtained with lower surface steps. BAE SYSTEMS [7], through their "AEROMEMS" research program (2000) concluded that MEMS-based fully developed flow control system could result in a timeframe of 10-15 years. [33]

Figure 1.7: Kline-Fogleman Modified (KFM)[35]

1.9 Airfoil and Wing Characteristics:

The primary lifting surface of an aircraft is its wing. The wing has a finite length called its wing span. If the wing is sliced with a plane parallel to the x-z plane of the aircraft, the intersection of the wing surfaces with that plane is called an airfoil. This airfoil shape can be different if the slice is taken at different locations on the wing. However, for any given slice, we have a given airfoil. We can now think of the airfoil as an infinitely long wing that has the same cross-sectional shape. Such a wing (airfoil) is called a two-dimensional (2-D) wing.[34]

Therefore, when we refer to an airfoil, we can think of an infinite wing with the same cross-sectional shape.

The National Advisory Committee for Aeronautics (NACA) did systematic tests on various shaped airfoils in order to generate a database for aircraft design. Although performed a long time ago, these data are still used when designing certain appendages of the aircraft. The system consists of a series of 4, 5, and 6 digit airfoils. [37] This was done by Eastman Jacobs in the early 1930s to create a family of airfoils known as the NACA Sections.

NACA Airfoils:

The NACA airfoils are airfoil shapes for aircraft wings developed by the National Advisory Committee for Aeronautics (NACA). Airfoils are described and can be distinguished between each other by the numbers that follow the acronym NACA. There are six NACA families which are 4- Digit, 5-Digit, 6-Series, 7-Series, 8-Series, and 16-Series. In NACA Four-Digit Series, four digits follow the acronym NACA and these 4 digits show 3 different properties of the airfoil. The first family of airfoils designed in the above-mentioned way is known as the NACA Four Digit airfoils. The explanation of the 4-digit NACA airfoil is as follows [41, 42]:

a. The first digit specifies the maximum camber in the percentage of the chord.

b. The second digit indicates the position of the maximum camber in tenths of the chord.

c. The last two digits provide the maximum thickness of the airfoil in percentage of the chord.

4-digit airfoils:

Symmetric airfoils in the 4-digit-series family are designated by a 4-digit number of the form NACA 00xx.The first two digits indicate a symmetric airfoil; the second two, the thickness-chord ratio.Ordinates for the NACA 4-digit airfoil family [11] are described by an equation of the form [43]

The constants in the equation were determined from the following boundary conditions:
Maximum ordinate:

$$\frac{x}{c} = 0.30 \qquad \frac{y}{c} = 0.10$$

$$\frac{dy}{dx} = 0$$

Ordinate at trailing edge:

Magnitude of trailing-edge angle: $\frac{x}{c} = 1.0 \qquad \left|\frac{dy}{dx}\right| = 0.234$

Nose shape: $\frac{x}{c} = 1.0 \quad , \frac{y}{c} = 0.078$

2 - maximum camber is 0.02% over the chord, 4 - the location of the maximum camber along the chord line given as 0.4 c 15 - the maximum thickness, here 0.15 c.For example, the NACA 2412 airfoil chosen for this paper has a maximum thickness of 12% with a camber of 2% located 40% back from the airfoil leading edge.[44]

Comparison of different digit airfoils:

Types	Merits	Demerits	Application
4-Digit	➢ Good stall characteristics ➢ Small center of pressure movement across a large speed range ➢ 3. Roughness has little effect	➢ Low maximum lift coefficient ➢ Relatively high drag ➢ 3. High pitching moment.	➢ General aviation ➢ Helicopter blades ➢ Missile/rocket fins.
5-Digit	➢ Higher maximum lift coefficient. ➢ Low pitching moment ➢ Roughness has little effect	➢ Poor stall behavior ➢ 2. Relatively high drag	➢ General aviation ➢ bombers, transports ➢ commuters ➢ Business jets
6-series	➢ Avoids low-pressure peaks ➢ Low drag at high speed	➢ Relatively low lift	➢ Aircraft propellers. ➢ Ship propellers.

High-Lift Devices:

High lift is rarely the only desirable aspect of an airfoil. The airfoil's lift-to-drag ratio, endurance parameter, thickness, pitching moment, stall characteristics, and sensitivity to rough- ness are all important factors, among others, that must each be weighed separately when one considers selecting or designing an airfoil. This study focuses on those factors that are most related to enhanced high-lift low Reynolds numbers airfoil performance. [10]

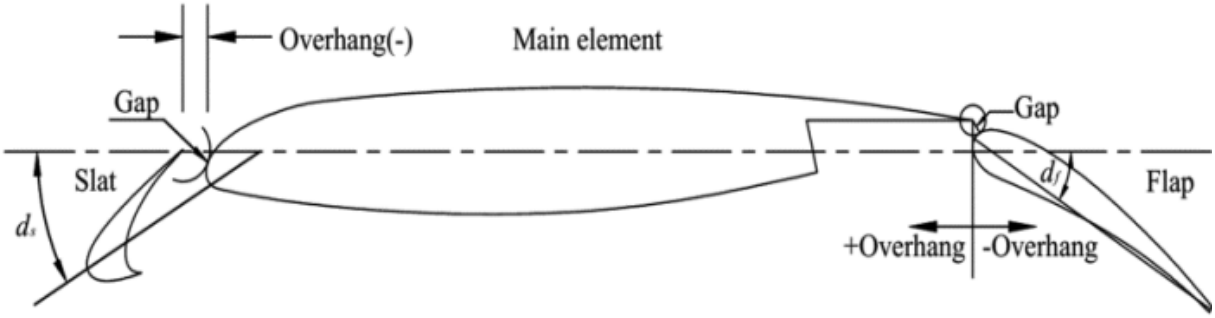

Figure 1.8 Multi Element Airfoil [11]

The baseline configuration of MDA three- element airfoil 30P30N, as shown in Fig.1.15, is used here as a validation case of numerical methods. Many efforts of multi-element airfoils computation have been made to various MDA three-element configuration, tested over the course of many years (primarily the 1990s) in the NASA Langley LTPT. For the 30P30N configuration with both slat and flap deflected 30°, the slat overlap and gap defined in Fig.1.15 are -2.50 and 2.95 percent of not deflecting airfoil chord, and the flap overlap and gap are 0.25 and 0.89 percent respectively.[66]

Modern aircraft use flaps and slats for high lift and increasing stall angle. In aircraft design and aerospace engineering, a high-lift device is a component or mechanism on an aircraft's wing that increases the amount of lift produced by the wing. The device may be a fixed component or a movable mechanism that is deployed when required. To achieve reasonable field performance while also obtaining efficient transonic cruise a fairly sophisticated hi**g**h lift system is required. Common movable high-lift devices include wing flaps and slats. Fixed devices include leading-edge root extensions and boundary layer control systems, which are less commonly used. [66]

<u>Flaps</u>:

Numerical results exhibited that the aerodynamic parameters of multi element airfoils with tail extending effect is much optimum than the standard NACA airfoils. [66] Flaps are high lift devices consisting of a hinged panel or panels mounted on the trailing edge of the wing. When extended, they increase the camber and, in most cases, the chord and surface area of the wing resulting in an increase of both lift and drag and a reduction of the stall speed. These factors result in an improvement in takeoff and landing performance increasing stall angle [34]

There are many different flap designs and configurations in use. Large aircraft sometimes incorporate more than one type, utilizing different flap designs on the inboard and outboard sections of the wing. The following are descriptions of some of the more common flap designs: [57]

- Plain Flap – The rear portion of the wing airfoil rotates downwards on a simple hinge arrangement mounted at the front of the flap. [56]

- Split Flap – The rear portion of the lower surface of the wing airfoil hinges downwards from the leading edge of the flap, while the upper surface remains immobile.
- Slotted Flap – Similar to a Plain Flap but incorporates a gap between the flap and the wing to force high-pressure air from below the wing over the upper surface of the flap. This helps reduce boundary layer separation and allows the airflow over the flap to remain laminar. [67]
- Fowler Flap – A split-flap that slides rearwards level for a distance before hinging downwards. It thereby first increases chord (and wing surface area) and then increases camber. This produces a flap that can optimize both takeoff (partial extension for the optimal lift) and landing (full extension for optimal lift and drag) performance. This type of flap or one of its variations is found on most large aircraft.
- Double Slotted Fowler Flap – This design improves the performance of the Fowler flap by incorporating the boundary layer energizing features of the slotted flap.[56]

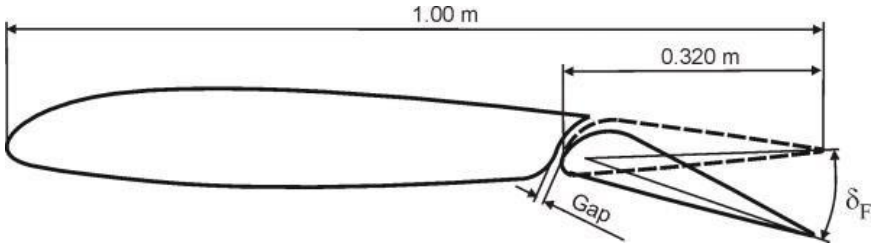

Figure 1.9 NACA 23012 airfoil with slotted flap [58]

In changing from a plain airfoil to an airfoil with flaps an increase of curvature of the airfoil is featured which gives part of the extra lift, but also depression is created which features a low pressure near the trailing edge. [55]

Slats:

Slats are extendable, high lift devices on the leading edge of the wings of some fixed-wing aircraft. Their purpose is to increase lift during low-speed operations such as takeoff, initial climb, approach, and landing. They accomplish this by increasing both the surface area and the camber of the wing by deploying outwards and drooping downwards from the leading edge.[52] In contrast, Krueger flaps increase wing camber by extending panels forward from the lower surface of the wing. Slats normally have several possible positions and extend progressively in concert with flap extension. Slats are most often extended and retracted using hydraulically or electrically powered actuators. In some more simplistic designs, however, they are held in the retracted position by aerodynamic forces and use springs or counterweights for an automatic extension at low speeds over high angles of attack.[68]

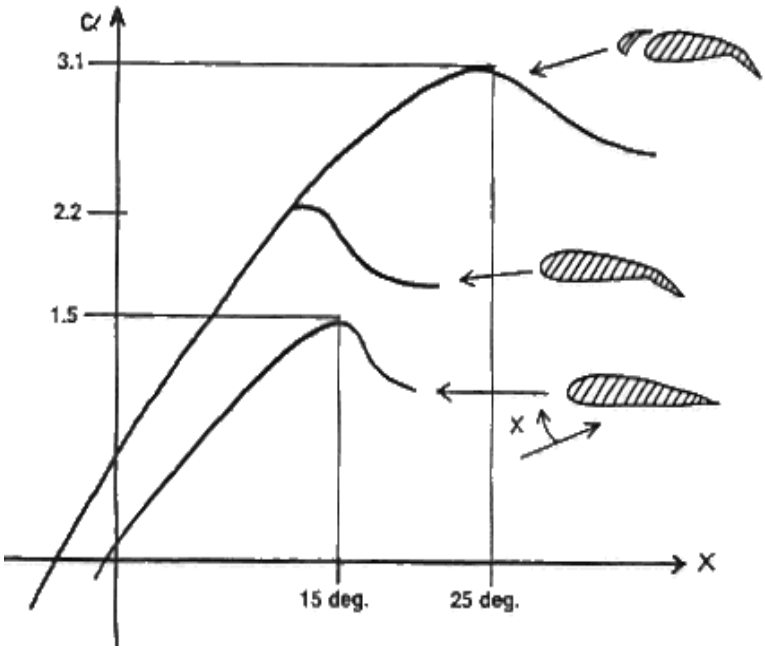

Figure: 1.10 Flaps and slats for high lift and increasing stall angle [55]

1.11 Wing Types

The wing is the primary lifting surface of an aircraft which sustains the weight of the aircraft to make the flight in the air while from an aerodynamics perspective it is also the main source of the aircraft drag. As a result, the effects of wing shape and size are crucial to aerodynamic characteristics on which the efficiency of aircraft depends. As such, researches on different wing shapes and geometries are still on throughout the world to explore the maximum possible lift and minimum possible drag. The present research is focusing on the improved aerodynamic characteristics and performance by reducing induced drag which is one of the primary sources of drag with the incorporation of various wingtip devices. [72] It is the most important structure of an airplane as it affects the cruise speed, takeoff and landing distances, stall speed, handling qualities (especially near the stall), and overall aerodynamic efficiency during all phases of flight. Lift is generated because there is a lower pressure on the upper wing surface and higher pressure on the lower wing surface. For a wing of finite span, this effect will cause the flow to pass from the low- pressure zone to the high-pressure zone at the wingtip as can be seen in Figure 1.16(a). This cross flow at the wingtip meets at the trailing edge and causes a wing-tip vortex. [15] Sometimes, the small extension at the wing tip is called a winglet and is placed at any angle to the existing wing surface so that the creation of rotating vortex flow at the wingtip is slowed down. A lift force is generated on the winglet due to the interaction of the winglet flow field and main wing flow field giving a forward component that can be seen as negative drag following the definition of drag and lift. This forward component of the lift force reduces the total wing drag. [16]

Rectangular Wing:

Such aircraft can carry a reasonable load and fly at a reasonable speed albeit does nothing superbly well. It is ideal for personal aircraft as it is a sinecure to control in the air as well as inexpensive to build and maintain. A heavily cambered rectangular wing (Aspect ratio around 6-8) with a blunt rounded leading edge will give good low-speed performance and very docile handling characteristics. Variations at this Reynolds range will be mainly in the amount of selected camber, depending on preferable speed range engine power. [18]

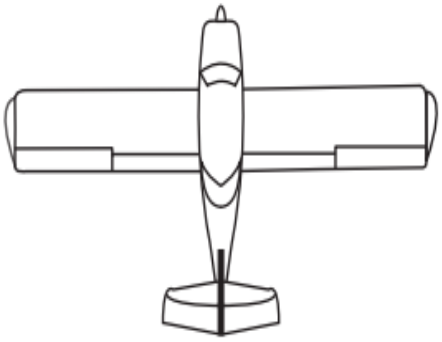

Figure 1.11 (a): 2D shape of rectangular wing [12]

Figure 1.11(b) Rectangular wing in P-51 Mustang [13]

Elliptical Wing:

The elliptical wing is similar to the rectangular wing and it excels in use on gliders, where its lengthy wingspan can capture the wind currents easily, providing lift without the need for a lot of forwarding momentum, or airspeed. An elliptical wing is a wing planform whose leading and trailing edges each approximate two segments of an ellipse. It should not be confused with annular wings, which may be elliptically shaped.[30]

Figure 1.12: 2D and 3D shape of Elliptical wing [12]

Relatively few aircraft have adopted the elliptical wing, an even-smaller number of which attained mass production; the majority of aircraft that did use this feature was introduced during the 1930s and 1940s. Perhaps the most famous aircraft to feature an elliptical wing is the Supermarine Spitfire, a Second World War-era British fighter aircraft. Another major application was the Heinkel He 70 "Blitz", a German fast mail plane and reconnaissance bomber; early versions of the He 111 bomber also used such a wing configuration before a simpler design was adopted for economic reasons.[8]

Figure 1.13: Super marine Spitfire uses a modified elliptical wing with NACA 2415 [13]

Swept Wing:

The swept wing is referred to as the “go-to” wing for jet-powered aircraft. It needs more forward motion to create lift than the rectangular wing, albeit producing much less drag in the system, meaning that the aircraft can travel faster. It works well at the higher altitudes, where most jet aircraft fly.[37]

Raked wing tip from Boeing Company was designed by Herrick and got the patent in 2000. The raked tip is attached with the main wingtip with a higher angle of sweep than the main wing. Boeing 777 long-range jets have been designed with a raked wingtip.[61]

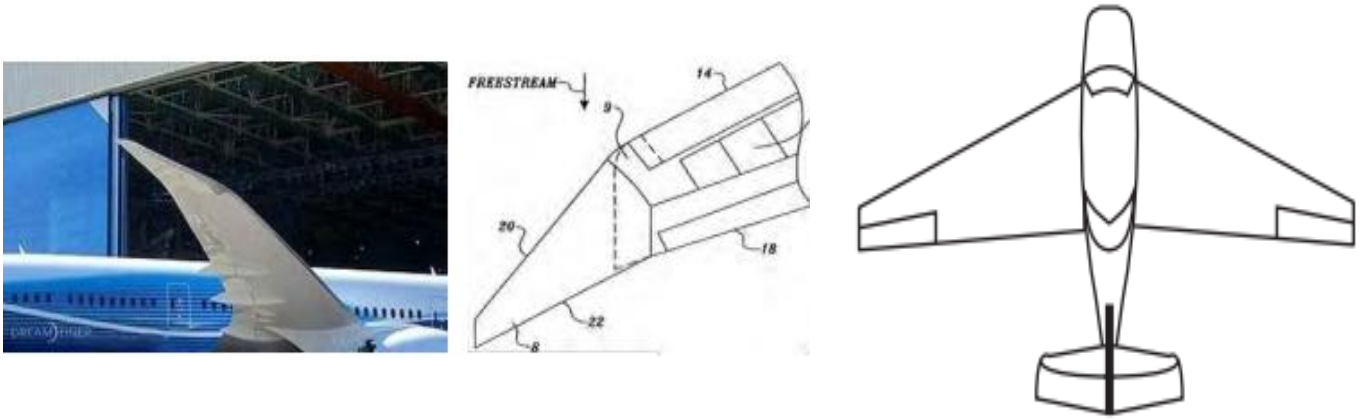

Figure 1.14. Raked Wing Tip and 2D shape of the swept wing [12]

NASA testified that forward swept wings can provide the benefits as of aft swept wings - decreasing the critical Mach number with Raked Wing Tip [14].

Figure 1.5 X-29 Backward swept wing [25]

Delta Wing:

The delta wing advances the swept-wing perception, pulling the wings even further back and creating even less drag. Nonetheless, the downside to this is that the aircraft has to fly extremely fast for this type of wing to be efficacious [37].

The unique design in the Blended winglet has no sharp edge at the wing/winglet intersection and is followed by a smooth curve. Aviation Partners Inc. (API) and Boeing Company made a collaboration in 1999 for the design of advanced blended winglets 1999. Mike Stowell, Executive vice president of APB mentioned the interference drag, an aerodynamic phenomenon caused due to the intersection of lifting surfaces, hence the winglet design was developed to overcome the interference drag formed at

the junction of wing and winglet. The winglets were retrofitted in Boeing business jets and also in B7371. Now, these flights have their services in American airlines (Southwest Airlines) and also in European airlines.[12]

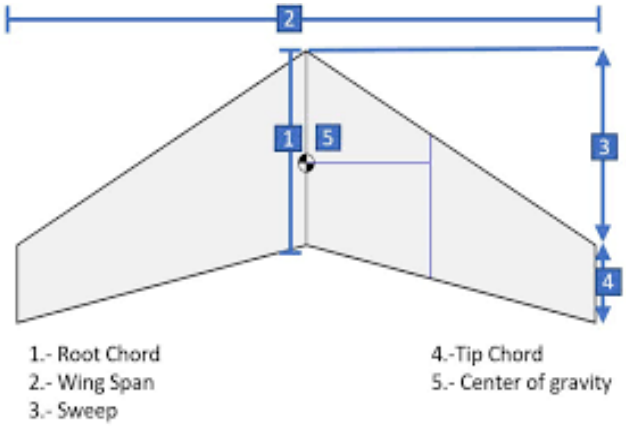

Figure 1.16 2D shape and Cross section of Delta wing [15]

Figure 1.17 Blended Winglet developed in Delta wing aircraft [12]

Ever since the winglet technology has been initiated, the merits were being investigated. Dr. Whitcomb has performed an experiment with the winglet in which the winglet shows reduction in drag about 20%. In 1977, Heyson made an experiment to study the advantages of Whitcomb's winglet. His results indicate that winglets would reduce the induced drag more than tip extension and will be at its best when it is nearly vertical [14].

Later in 1980, Jones et al made a research in winglets to determine its effect over the induced drag using Trefftz-plane theory and concluded that the vertical length of the winglet should be twice than the length of horizontal extension in order to have its gain over tip extension. [16]

Supercritical wing:

Another new tailoring of an airfoil design was the supercritical wing which delayed the formation and reduced the strength of the shock wave over the wing just below and above the speed of sound impeding the formation of shock wave formation at these high speeds resulting in less drag. Results of NASA [17] supercritical wing research showed that aircraft using the concept would have increased cruising speed, improved fuel efficiency, and greater flight range. Supercritical wings are now commonplace on virtually every modern subsonic commercial transport. [30]

Figure 1.18 Supercritical jet developed by NASA [13]

The unprecedented design of the Supercritical Wing decreases the effect of shock waves on the upper surface near Mach 1, which in turn lessens drag.

Table 1 Some essential features of swept wing and delta wing aircrafts

The following table shows Some essential features of swept wing and delta wing.[30]

S. no.	Name of the aircraft	Crew	Wing area (m^2)	Empty weight (kg)	Loaded weight (kg)	Aspect ratio	Power plant	Height(m)
							Dry thrust(KN)	
1	Grumman f-14 tomcat	2	54.5	19838	27,700	2.5	61.4	4.88

2	General dynamic f-111f	2	48.77	21400	37600	1.95	79.6	5.22
3	Panavia tornado	2	26.6	13890		7.2	43.8	5.95
4	Sukhoi su-17	1	34.5	12160	18400	3.5	76.4	5.12
5	Mig-23 mcd flogger-k	1	34.16	9595	15700	5.7	83.6	4.82
6	Dassault mirage f-1	1	25.00	7400	10900	2.8	49.03	4.50
7	MC donnell douglas f4 phantom ii	2	49.2	13757	18825	2.8	52.9	5.0
8	Sukhoi Su-24	2	55.2	22300	38040	1.9	75	6.19
9	Vought xf8u-3 crusader-iii	1	41.8	9915	14660	3.5	73.4	4.98
10	English electric lightning	1	44.01	14092	18638	2.5	55.74	5.97
11	Mikoyan-Gurevich mig-17F	1	22.6	3919	5350	4.1	22.5	3.80
12	Chengdu j-7MG	1	24.88	5292	7540	2.8	44.16	4.11

Working data:

Name of the aircraft	Cruise speed(km/hr)	Range(km)	Service ceiling(m)	Thrust/ weight	Rate of climb(m/s)	Wing loading (kg/m^2)
Grumman f-14 tomcat	2235	2960	25,200	.92	229	508.25
General dynamic f-111f	2655	6760	20000	0.61	131.5	771.96
Panavia tornado	2400	3890	15240	0.55	76.7	707.95
Sukhoi su-17	1460	2300	14200	0.68	230	533.33
Mig-23 mcd flogger-k	2425	2820	18500	0.88	240	434.18
Dassault mirage f-1	2538	3300	20000	0.67	243	436
MC donnell douglas f4 phantom ii	2437	2600	18300	0.86	210	416.48
Sukhoi su-24	1154	2775	11000	0.60	150	689.13
Vought xf8u-3 crusader-iii	1225	3290	19800	0.74	165	351
English electric lightning	2102	2040	12000	0.78	100	423.49
Mikoyan-gurevich mig-17F	1445	2060	11600	0.63	65	236.72

Initial Data visualization of these parameters concerning speed:

Cruise speed(km/hr)	With After burner thrust (KN)
2485	223.7
2655	112
2400	76.8
1860	109.8
2415	127
2338	70.6
2470	89.4
1554	109.8
1325	131.2
2101	71.17
9545	33.8
2200	64.7

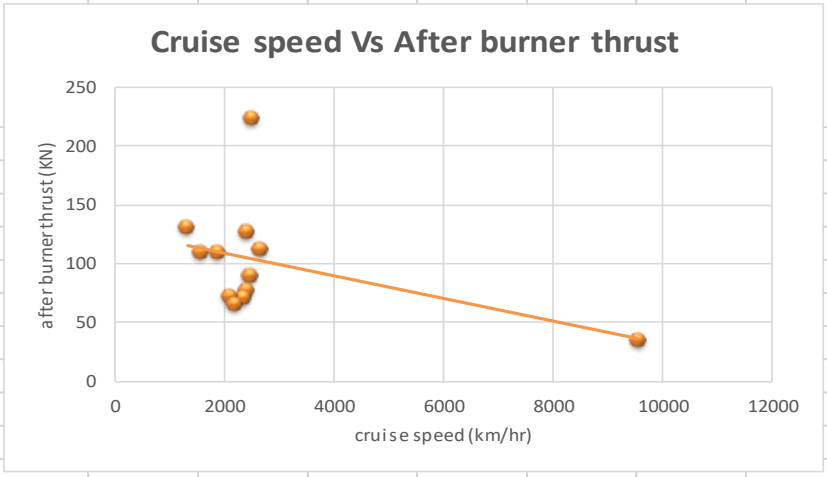

Fig. a Cruise speed vs. After burner thrust.

Cruise speed(km/hr)	Service ceiling(m)
2485	15,200
2655	20100
2400	15240
1860	14200
2445	18500
2338	20000
2370	18300
1654	11000
925	19800
2100	16000
1145	16600
2200	17500

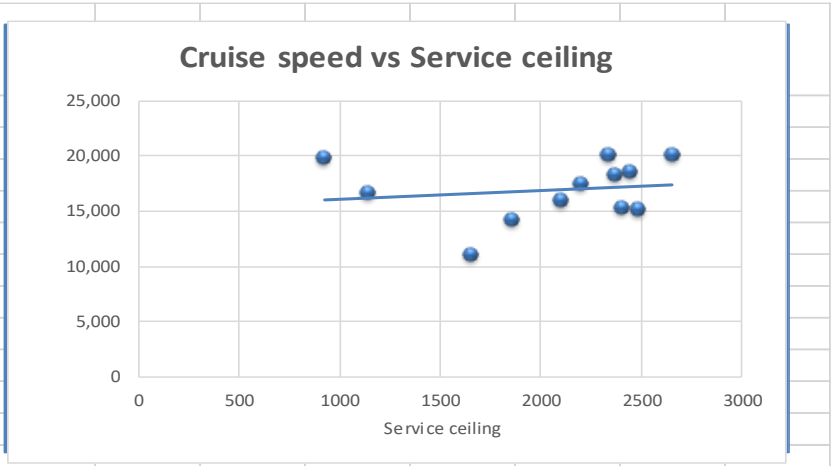

Fig b. Cruise speed vs. service ceiling.

Cruise speed(km/hr)	Wing loading(kg/m^2)
2435	598.25
2635	721.96
2500	721.95
1960	234.33
2415	924.18
2338	582
2470	816.48
1554	900
1325	751
2101	576.433
9345	226.72
2200	323.05

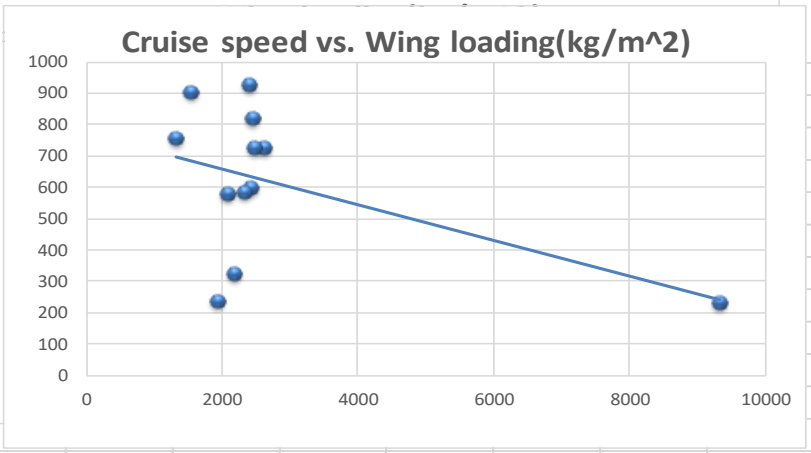

Fig. c Cruise speed vs Wing loading

Cruise speed(k	Wing area (m^2)
2485	54.34435
2655	42.77
2400	22.12
1860	33.5
2415	50.16
2338	45
2470	98.2
1554	83.2
1325	51.8
2101	41.01
9545	21.6
2200	29.88

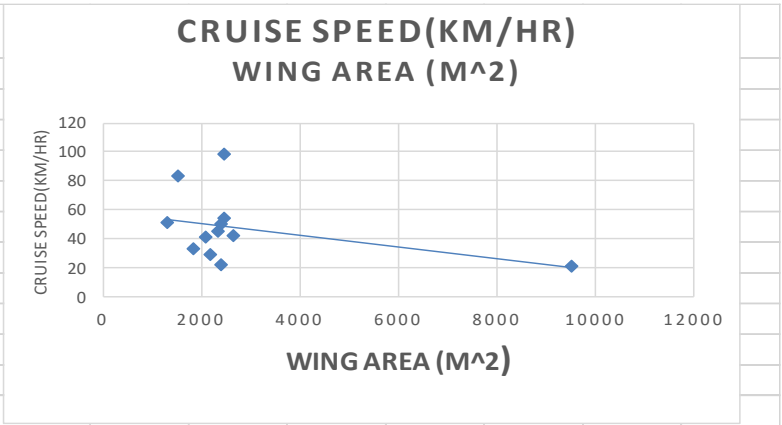

Fig. d Cruise speed vs. Wing Area.

Cruise speed(km/hr)	Dry thrust(KN)
2485	61.4
2655	79.6
2400	43.8
1860	76.4
2415	83.6
2338	49.03
2470	52.9
1554	75
1325	73.4
2101	55.74
9545	22.5
2200	44.16

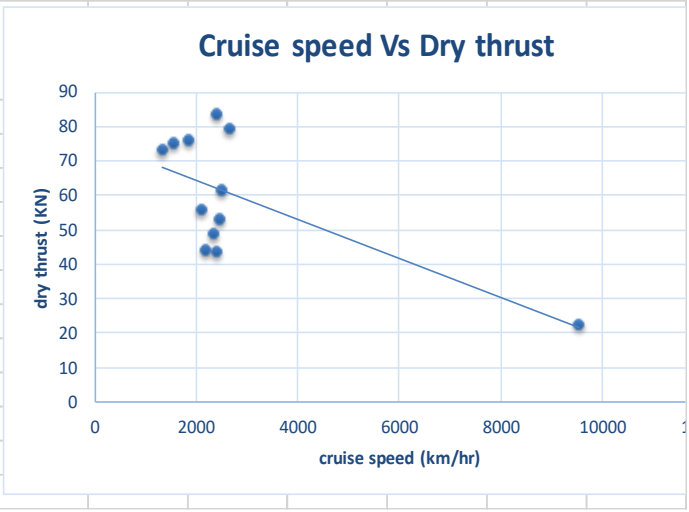

Fig. e. Cruise speed vs Dry thrust.

Just as much as most other things in life have compromised, it is no different in the case of wing design. While each design works well, all of these also have limitations making them efficacious only for certain task.

Chapter 2

Airfoil geometry

2.1 Symmetrical Airfoil

Airfoil geometry can be characterized by the coordinates of the upper and lower surface. It is often encapsulated by a few parameters such as maximum thickness, maximum camber, the position of max thickness, the position of max camber, and nose radius. One can generate a reasonable airfoil section given these parameters. [30]

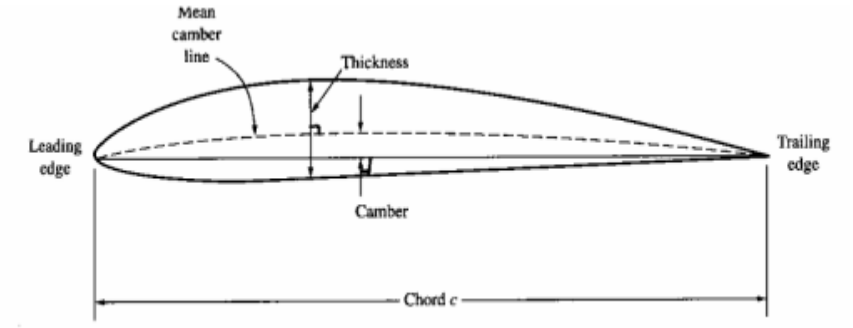

Figure 2. Geometrical shape of Airfoil [19]

The aerodynamic performance of airfoil sections can be studied most easily by reference to the distribution of pressure over the airfoil. Although specific examples can be cited in which each of the principles predict and contribute to the formation of lift, lift is a complex subject.[36] The production of lift is much more complex than a simple differential pressure between upper and lower airfoil surfaces. In fact, many lifting airfoils do not have an upper surface longer than the bottom, as in the case of symmetrical airfoils. These are seen in high-speed aircraft having symmetrical wings, or on symmetrical rotor blades for many helicopters and wind turbines whose upper and lower surfaces are identical. [45] In both examples, the only difference is the relationship of the airfoil with the oncoming airstream (angle).The following data has 96 values with different airfoil parameters for a Symmetric airfoil. [25]

The following dataset is calculated for: NACA 0012 airfoil at Reynold's number 50,000. [75]

NACA 0012 Reynold's Number = 50,000

There are 96 rows in this dataset. L/D has been calculated for each row .All the other datasets in this paper are compressed in the same way.

Table 2 **NACA 0012 Reynold's Number = 50,000**

Data visualization

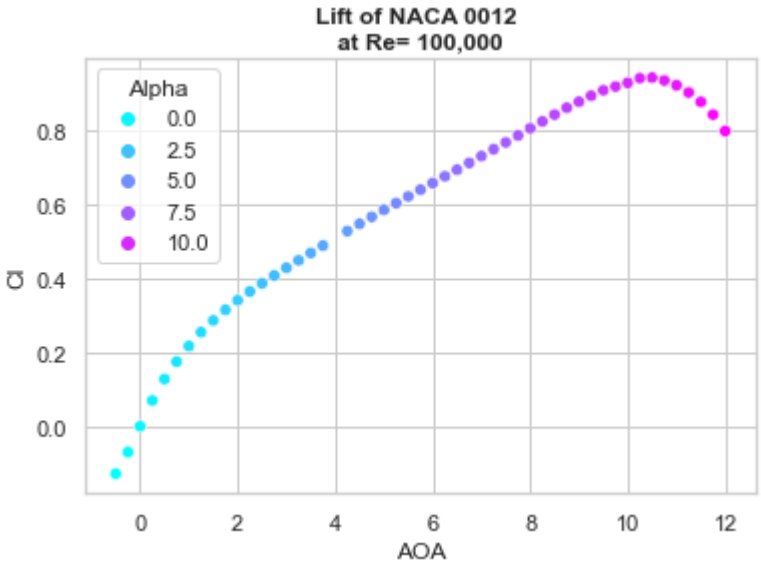

Figure 2.1 Lift vs AOA

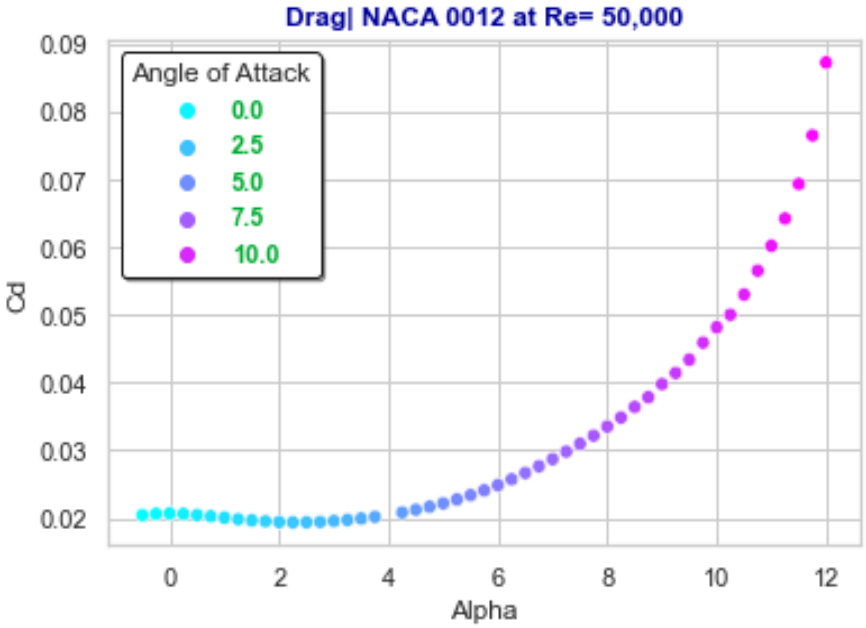

Figure 2.2 Drag vs. Angle of attack.

It is evident that stall angle is at 11 degree and the best ratio between Cd and Cl occurs when α achieves about 4-5 degrees for NACA 0012 the Reynolds number Re = 50,000.

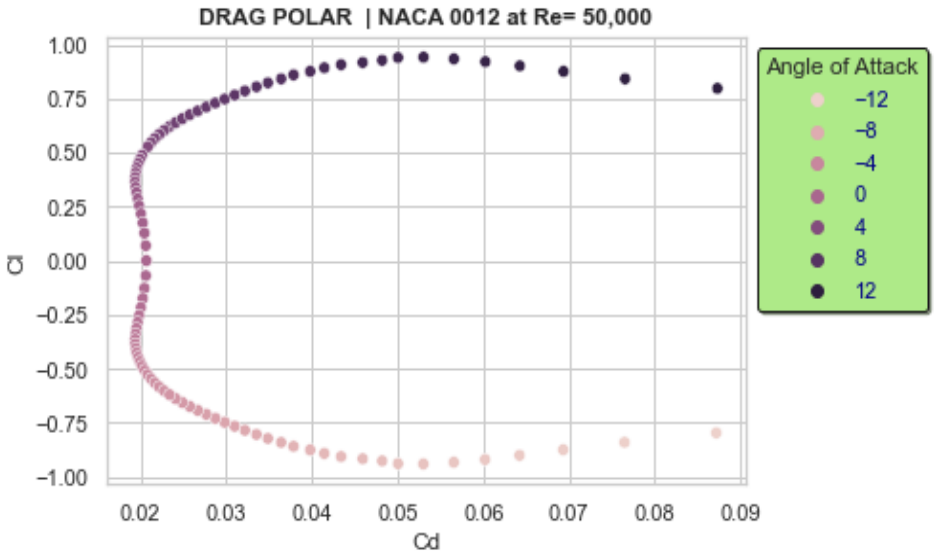

Figure 2.3 Drag polar(C_l vs. C_d)

In aerodynamics, the main source of the airplane drag is related with the wing. Around two-thirds of the total drag of typical transport aircraft at cruise conditions is produced by the wing [2]. There are three sources of drag:

(i) profile drag which is related to skin friction caused by flow of air over the aircraft surface

(ii) induced drag which is the result of lift generation for finite wingspan and

(iii) the compressibility drag caused by high speed aerodynamics.

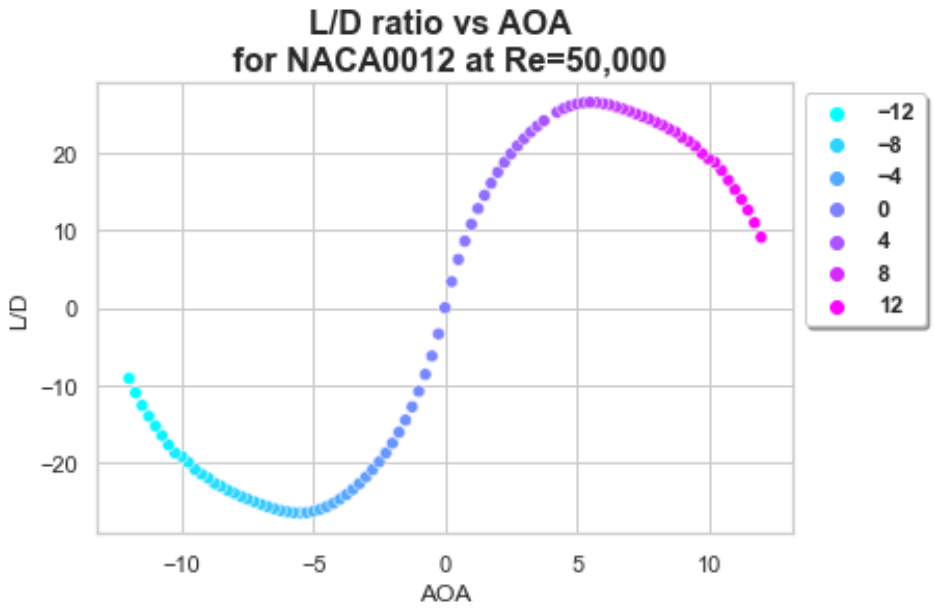

Figure 2.4 L/D vs. Angle of attack

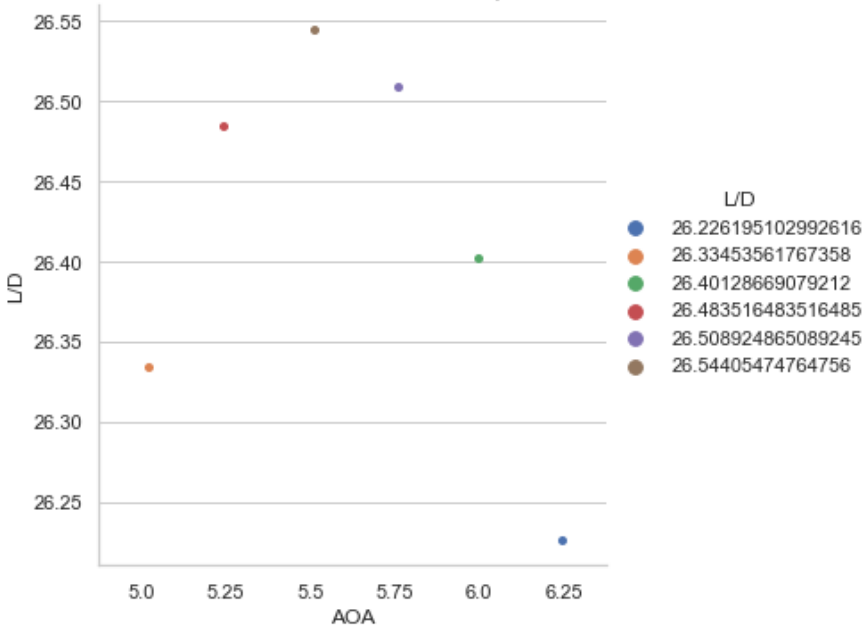

Figure 2.5 Max. L/D

Fig. 2.5 is the close observation to the high curve of figure 2.4 which confirms that L/D is high at about 5-6 degrees.

So, Efficient AOA is at about 5.5 degrees at Re= 50,000.In this AOA L/D is about 27 (approx.) from dataset by calculating (Cl/Cd). Also oitching moment should be reained below 0-5 degrees.

Figure 2.6(a) AEROBATIC AIRCRAFT use NACA 0012 Airfoil [13]

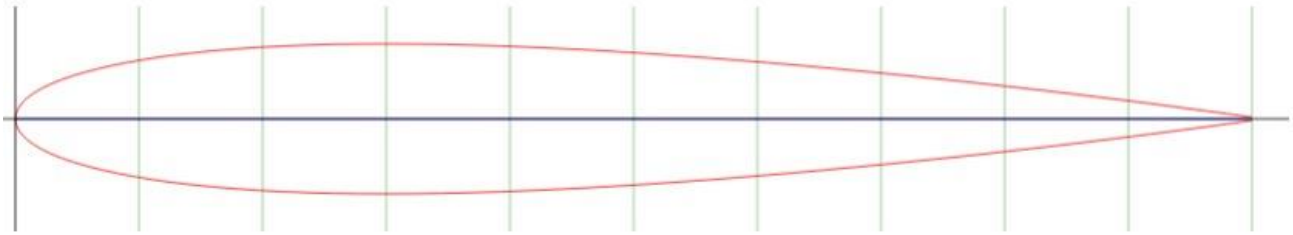

Figure 2.6(b) NACA 0012 cross sectional shape [76]

As an airfoil moves through the air, the airfoil is inclined against the airflow, producing a different flow caused by the airfoil's relationship to the oncoming air. A hand being placed outside the car window at a high speed. If the hand is inclined in one direction or another, the hand will move upward or downward. This is caused by deflection, which in turn causes the air to turn about the object within the air stream [28]. As a result of this change, the velocity of the object changes in both magnitude and direction, in turn resulting in a measurable velocity force and direction. For the pressure distribution of an airfoil, we essentially plot C_p vs. x/c where x/c varies from 0 at the leading edge to 1.0 at the trailing edge. C_P is plotted "upside-down" with negative values (suction), higher on the plot. (This is done so that the upper surface of a conventional lifting airfoil corresponds to the upper curve.) The C_P starts from about 1.0 at the stagnation point near Various parts of the pressure distribution are represented in the figure below and are interpreted in the following sections:[40]

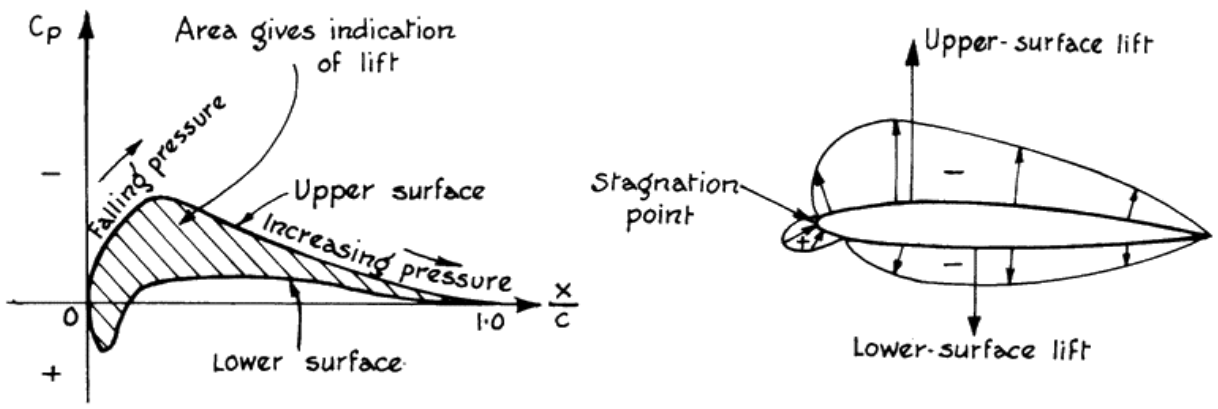

Figure 2.6. Pressure distribution around an airfoil [40]

In this figure, the static pressure on both surfaces will be less than atmospheric pressure, and thus will produce a lifting force on both upper and lower surfaces. The important point is the difference in the pressures produced. The static pressure on the upper surface will be less than the static pressure on the lower surface, creating a pressure differential. The lower static pressure on the upper surface will pull the wing upward, creating a lifting force [39].

If pressure is applied to an area, a force is generated. The pressures acting on an airfoil are the result of the dynamic pressure the airfoil is experiencing. Experiments have shown that the aerodynamic force equation can be written as the product of dynamic pressure (q), the surface area of the airfoil (S), and a variable C_F, called the coefficient of aerodynamic force. The coefficient represents the shape and orientation of the surface area within the relative wind.[40]

$$AF = qSC_F = \frac{1}{2}\rho V^2 S C_F$$

Hence, lift and drag are the perpendicular and parallel components of aerodynamic force, they are functions of the same factors: Wing area, dynamic pressure and a coefficient. The equations for lift and drag are:

$$L = qSC_L = \frac{1}{2}\rho V^2 S C_L$$

$$D = qSC_D = \frac{1}{2}\rho V^2 S C_D$$

Angle of Attack: The angle between the chord line and the relative airflow. Angle Of Attack is the most important factor in the coefficient of lift as this is the most sinecure job for the pilot to govern. The angle of incidence is the angle between the longitudinal axis and the relative airflow and this is the angle that is fixed and cant be altered.[40]

Upper Surface:

The upper surface pressure is lower (plotted higher on the usual scale) than the lower surface C_p in this case. [40]

Lower Surface :The lower surface sometimes carries a positive pressure, but many design conditions are pulling the wing downward. In this case, some suction (negative C_p > downward force on lower surface) is present near the mid-chord. [38]

Pressure Recovery :

This region of the pressure distribution is called the pressure recovery region. The pressure increases from its minimum value to the value at the trailing edge. This area is also known as the region of an adverse pressure gradient. As discussed in other sections, the adverse pressure gradient is associated with boundary layer transition and possibly separation, if the gradient is too severe. [40]

Trailing Edge: Pressure The pressure at the trailing edge is related to the airfoil thickness and shape near the trailing edge. For thick airfoils, the pressure here is slightly positive (the velocity is a bit less than the freestream velocity). For infinitely thin sections Cp = 0 at the trailing edge. Large positive values of C_p at the trailing edge imply more severe adverse pressure gradients. [16]

C_L and C_P:

The section lift coefficient is related to the C_P by C_L = int (C_{pl} – C_{pu}) dx/c (It is the area between the curves.) with C_{pu} = upper surface C_P and recalls C_l = section lift / (q/c) [27]

Stagnation Point:

The stagnation point occurs near the leading edge. It is the place at which V = 0. Note that in incompressible flow C_p = 1.0 at this point albeit incompressible flow it may become larger.

Any section of the wing cut by a plane parallel to the aircraft xz plane is called an airfoil. It usually looks like a positive cambered section that the thicker part is in front of the airfoil. An airfoil-shaped body moving through the air will vary the static pressure on the top surface and the bottom surface of the airfoil.[27]

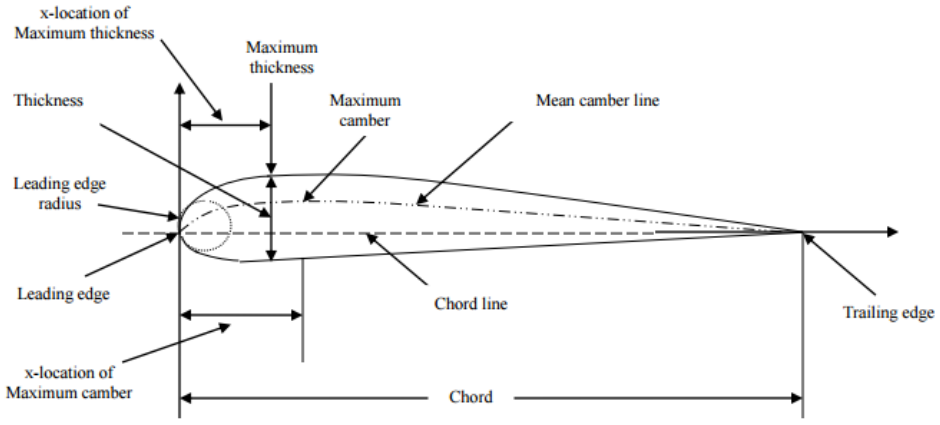

Figure 2.7 A Cross sectional shape of NACA 2412 Airfoil [50]

If the mean camber line is straight, the airfoil is referred to as symmetric, otherwise, it is called a cambered airfoil. The camber of an airfoil is usually positive. In a positive cambered airfoil, the upper surface static pressure is less than surrounding pressure, while the lower surface static pressure is higher than surrounding pressure. This is due to higher airspeed at the upper surface and lower airspeed at a lower surface of the airfoil. As the angle of attack is incremental, the pressure difference between upper and lower surfaces will be incremental.[60]

- Chord length (c) – length from the leading edge to the trailing edge of a wing cross-section that is parallel to the vertical axis of symmetry.
- Mean camber line – the line halfway between the upper and lower surfaces.
- Leading-edge (LE) – is the front-most point on the mean camber line. trailing edge (TE) – This is the most rearward point on the mean camber line.
- Camber – the maximum distance between the mean camber line and chord line, measured perpendicular to the chord line. The airfoil is symmetric above and below the chord line[60]

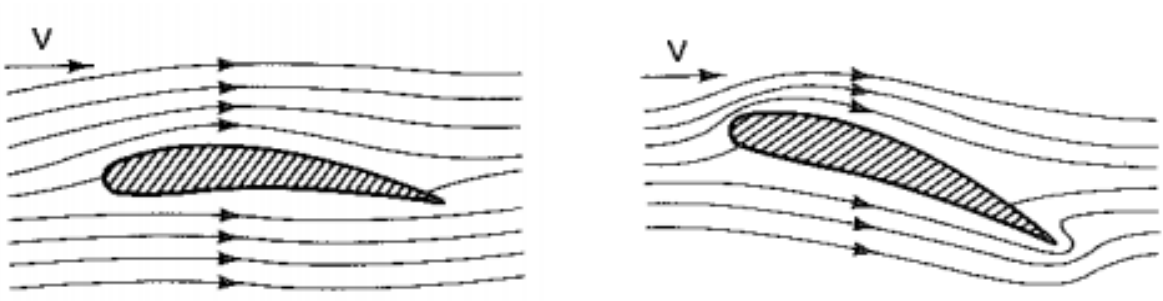

a. Small angle of attack *b. Large angle of attack*

Figure 2.8 Air circulation around the airfoil in individual AOA [22]

DYNAMIC STALL:

A dynamic stall is a condition of flight where an increase in AOA has resulted in a decrease in C_L . In Figure, we see that C_L increases linearly over a large range of angles of attack then reaches a peak and begins to ·decrease. The highest point is C_{LMAX} and any increase in AOA beyond C_{LMAX} AOA produces a decrease in C_L. Therefore, C_{LMAX}AOA is known as the stalling angle of attack or critical angle of attack, and the region beyond C_{LMAX} AOA is the stall region. [20]

$$V_s = \sqrt{\frac{2W}{\rho S C_{Lmax}}}$$

Stall speed (V_s) is the minimum true airspeed required to maintain level flight at C_{LMAX} AOA. Although the stall speed may vary, the stalling AOA remains constant for a given airfoil. Since lift and weight are equal in equilibrium flight, we can substitute weight (W) for lift (L) in the lift equation. By solving for velocity 01), we derive a basic equation for stall speed. By substituting the stall speed equation into the true airspeed equation and solving for indicated airspeed, we derive the equation for the indicated stall speed. Weight, altitude, power, maneuvering, and configuration greatly affect an airplane's stall speed.[22]. Stalls result in decreased lift, increased drag, and an altitude loss. They are particularly dangerous at low altitude or when allowed to develop into a spin. The only action necessary for stall recovery is to decrease the AOA below C_{LMAX} AOA.[33]

2.3 Stall detectors:

Numerous devices may give the pilot a warning of an approaching stall. They include AOA indicators, rudder pedal shakers, stick shakers, horns, buzzers, warning lights and electronic voices. Some of these devices receive their input from attitude gyros, accelerometers, or flight data computers, but most receive input from an AOA probe. The AOA probe is mounted on the fuselage or wing and has a transmitter vane that remains aligned with the relative wind. The vane transmits the angle of attack of the relative wind to a cockpit AOA indicator or is used to activate other stall warning devices. Most USN and many USAF airplanes have standardized AOA indicators graduated in arbitrary units angle of attack, or graduated from zero to 100 percent.[22]

Stall warning in the T -37 is accomplished with aerodynamic stick shakers. The turbulent airflow caused by the separation of the boundary layer moves aft and hits the elevator causing it to shake and vibrate. This buffeting is the pilot's warning of an approaching stall. If the flaps are down, the turbulent airflow will pass beneath the elevator without causing buffeting. .[22] To correct this problem, small spoilers are located on the upper surface of the engine nacelles. This spoiler system works well except when the aircraft is configured and above approximately 90 KIAS. During these accelerated stall conditions, the spoilers don't extend. However, if the· speed brake is out, a light to moderate natural buffet is produced prior to the stall. Any further increase in angle of attack will cause the aircraft to abruptly stall. If the speed brake is not used and the flaps are extended 50 to 100 percent, there will be an approach to stall warninng. This stall is accompanied with a rapid onset of airframe buffeting occurring simultaneously with a stagnation of the nose trailing edge that pulls the air around the leading edge which impedes the separation.[28]

Chapter 3

Airfoils of wind turbines

A wind turbine is a rotary device that extracts kinetic energy from the wind. It has rotor blades mounted on the shaft which is connected to the generator through transmission devices. The blade profiles play an important role which decides the performance of the wind turbine. [49]

For the effective energy extraction, blades of modern wind turbine are made with airfoil sections. Major features of such an airfoil are shown in Fig1.4The airfoils used for the earlier day's wind turbines were the aviation air foils under the NACA (National Advisory Committee for Aeronautics) series. NACA specifies the features of the airfoil by numbers.[54]

The first wind turbine blades were also designed by the airfoils from aeronautic applications. However, in the 1980s, the airfoils specially dedicated for wind turbines were begun to be made due to the defects of aeronautic airfoils applied in a wind turbine. The sensitivity roughness effect on the leading edge arose to be the required element for wind turbine airfoil. The airfoil series for a stall-regulated, variable-pitch control wind turbine was developed by NREL in 1984, incorporated with SERI and airfoils [20] by the team of the Delft University of Technology with the design objective of low sensitivity to roughness, Gurney flaps, and trailing-edge wedge consideration. The airfoils from rising were designed to have high aerodynamic efficiency and slender blade shape.[51] The airfoil design using numerical optimization for the tip region of the blades was researched by Grasso. As mentioned in these studies, the higher aerodynamic efficiency, insensitivity to roughness effect, structural stability and smooth post-stall exhibition, etc., are required for wind turbine airfoil design. To accomplish these objectives, boundary layer consideration of the wind turbine airfoil can be conducive as it was proven from the laminar airfoil by Jacobs [20].

Working process of wind turbines: There are many ways to convert the wind kinematic energy into mechanical work or electricity. We can classify wind energy converters according to their aerodynamic function and constructional design. The aerodynamic function of the rotor is capturing wind energy and we can qualify it in two main ways.[39] The first method captures wind energy exclusively from aerodynamic drag of the air stream acting on the rotor surface. The second way uses the aerodynamic lift created by the flow against suitably shaped surfaces. It should be noted that the drag-type rotor is the oldest design of wind rotors [42] and its efficiency is lower than in the case of the lift-type rotor. [40].

The classification according to the constructional design of wind turbines is more figurative and obvious for everyone. The most important part of this characteristic is the direction of a rotor's axis of rotation. The axis can be directed horizontally (Horizontal Axis Wind Turbine – HAWT) or vertically (Vertical Axis Wind Turbine – VAWT) [50]. So, There are mainly two types of wind turbine.

The Horizontal Axis Wind Turbines have a horizontal rotor shaft and an electrical generator which is both located at the top of a tower.[54]

The Vertical Axis Wind Turbines – abbreviated as VAWTs, are designed with a vertical rotor shaft, generator and gearbox which are placed at the bottom of the turbine, and a uniquely shaped rotor blade that is designed to harvest the power of the wind no matter which direction is it blowing. The first is the **Darrieus wind turbine,** which is designed to look like a modified egg beater.

These turbines have very good efficiency, but poor reliability due to the massive amount of torque which they exert on the frame. Furthermore, they also require a small generator to get them started[42].

Figure 3.1 several applications of small scale VAWT [41]

The shape of a blade rotor is similar to an airplane wing airfoil. In both cases, suitably shaped surfaces produce a lift force, but that force is used for different purposes. [53]
Over the past decade, commonly used airfoil families for horizontal axis wind turbines (HAWTs) have included the NACA 44XX, NACA 23XXX, NACA 63XXX, and NASA LS series airfoils. Variable-pitch toward stall would result in similar roughness losses as fixed pitch, stall-regulation, while variable-pitch toward feather would decrease the loss to around 10% at the expense of the rotor being susceptible to power spikes in turbulent high winds. For variable-rpm rotors operating at constant tip-speed ratio and angle of attack distribution, the loss is minimal at around 5% to 10%. To minimize the energy losses due to roughness effects and to develop special purpose airfoils for HAWTs, the National Renewable Energy Laboratory (NREL), formerly the Solar Energy Research Institute (SERI), and Airfoils Inc. began a joint airfoil development effort in 1984. Results of this effort are reported in [25, 26].

Table 3 **HAWT S809 and S813 at Reynold's Number = 50,000[78]**

Airfoil NREL S809 And NREL S813 are selected for the optimization. The blades are simulated at a different angle of attack at different air velocities.

Mach Number =0

Reynold's number= 100,000

Airfoil name : NREL S809 and S813.

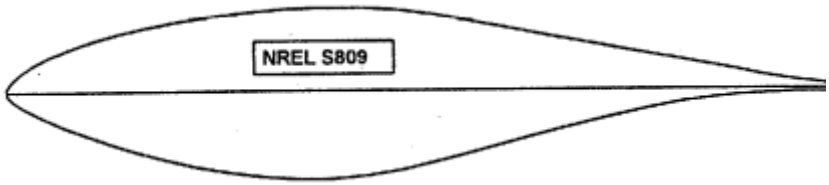

Figure 3.4(a) NREL S809 (PRIMARY OUTBOARD AIRFOIL, 75% RADIUS) [25]

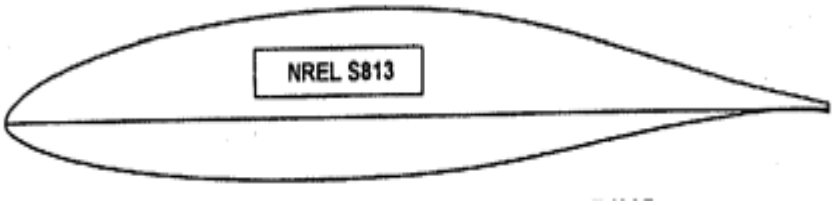

Figure 3.4(b) NREL S813 (TIP-REGION 95% RADIUS) [26]

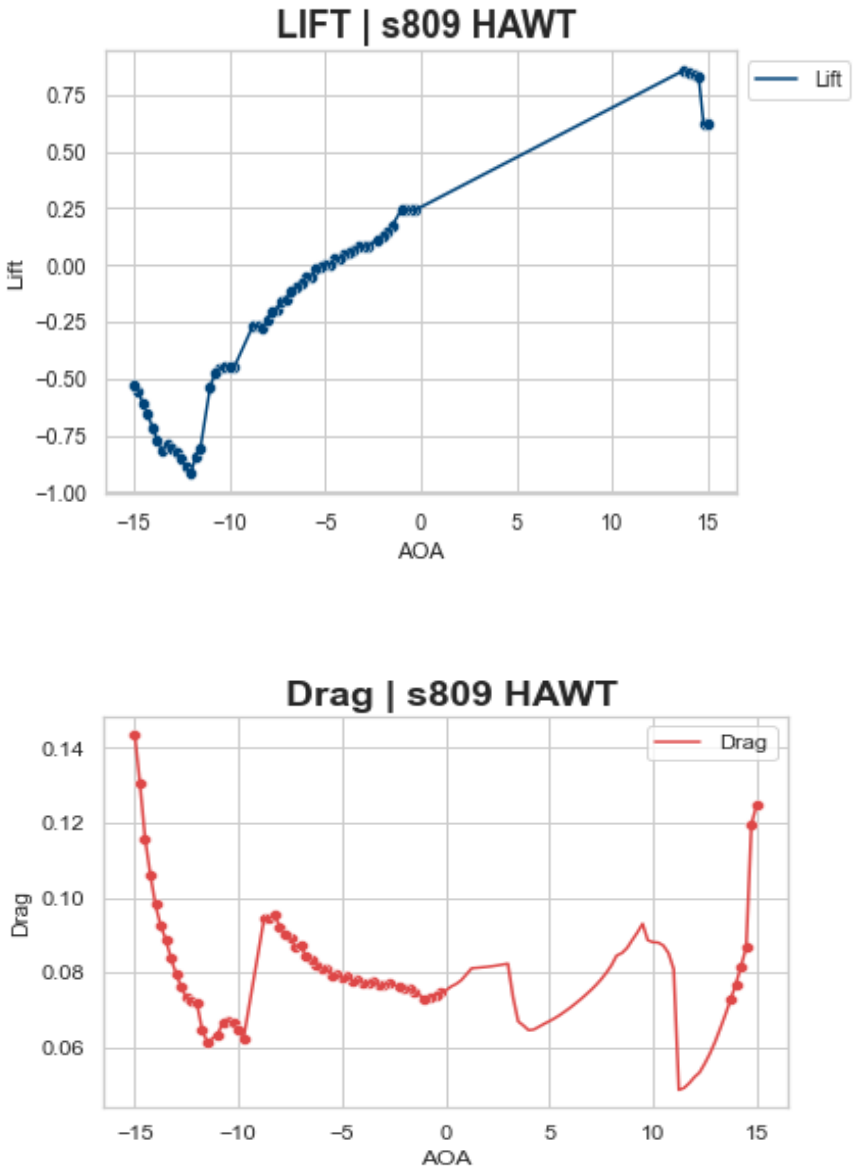

Figure 3.5 Lift, Drag vs. AOA for NREL S809

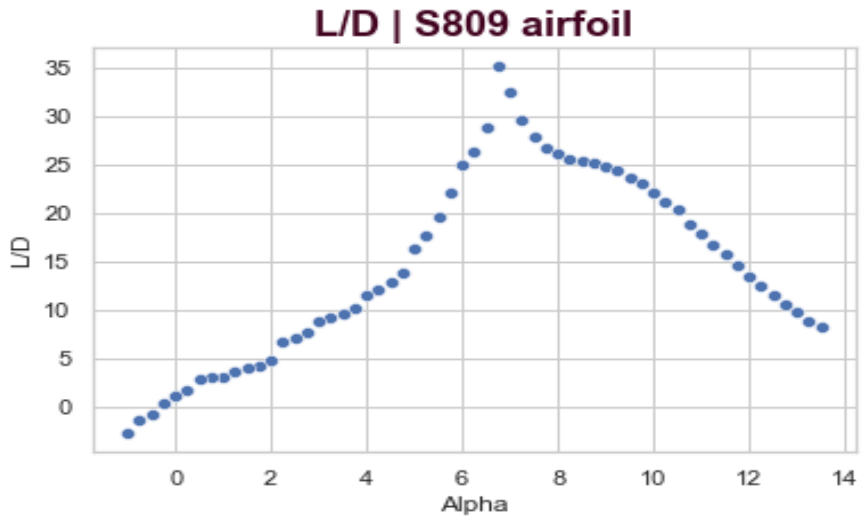

Figure 3.6 L/D vs. Angle of attack

A close look at the angle 4-6 degrees of this curve (Fig 3.6) can find the efficiency of the L/D variables at the specific AOA So, Efficient AOA is at about 6.75. Maximum L/D is 36(approximately) at Reynold's number= 50,000. In order to maximize the aerodynamically induced torque, an s890 rotor with pitch control is needed. This solution allows for controlling the value of the AOA to achieve higher values of the lift force at smaller AOA. Comparing with a corresponding airfoil **NREL-s813** airfoil we can look at the efficiency separately. Fig. 3.7 shows the difference in angle of attack of S809 and S813 at the max. Cl/Cd ratio.

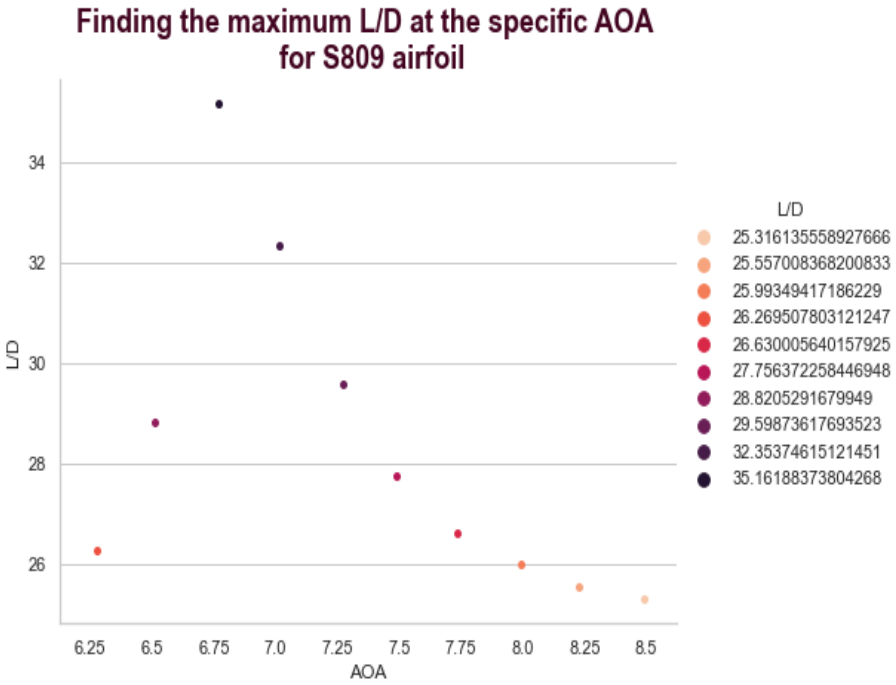

Figure 3.7 Max. L/D vs. Angle of attack

Comparing this airfoil with the corresponding S813 airfoil, some variations in lift and drag is observed:

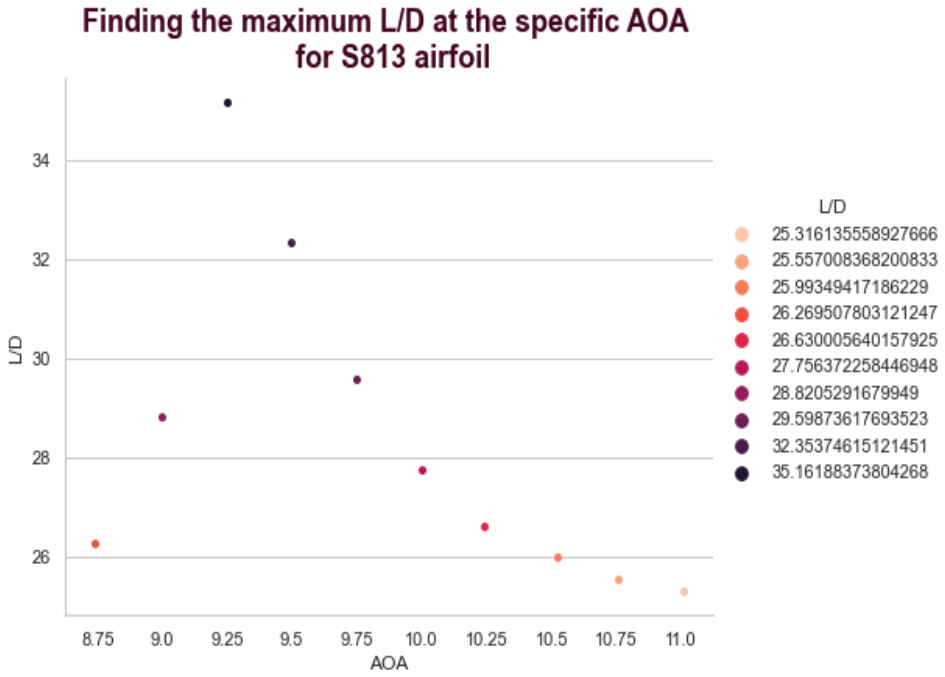

Figure 3.8 L/D vs. Angle of attack

It is evident that L/D is maximum at higher AOA 9.25 degs in **NREL- S813** comapring with **NREL- S809** at 6.75 degrees. L/D ratio is 35(approx.) in the both the cases.

The coefficient of Drag and Lift For airfoil NREL S809 and NREL S813 for the angle of attack from 0 to 25 degree and 15m/s,30m/s velocity. NRELS809 and NREL S813 is showing different Coefficient of Drag and Lift at low velocity 15m/s and high velocity 30m/s airfoil NREL S813 has maximum lift and minimum drag compare with NREL S809. [54]

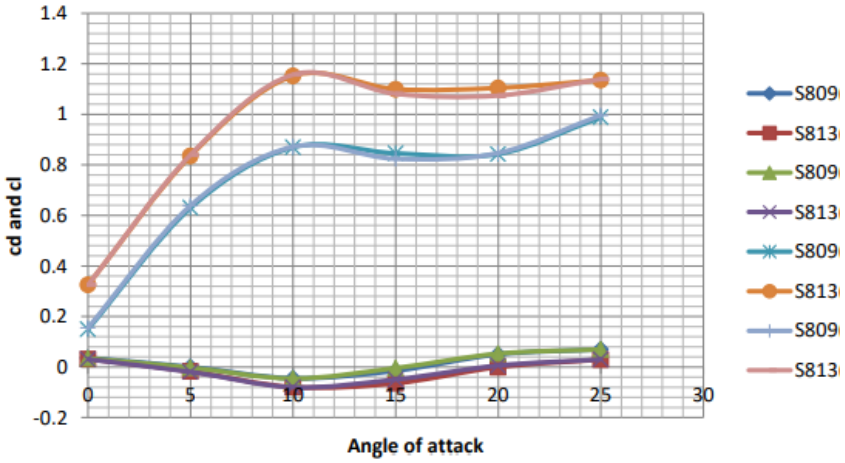

Figure 3.9 Lift, Drag vs Angle of attack

Different color of curve shows the maximum and minimum coefficient of drag and lift. Thus the design angle for both blades should be between 7 degrees to 10 degrees for better structural performance·

Figure 3.10: NREL-S809 airfoil developed in HAWT model [69]

Properties of VAWT :

The main advantage of the vertical axis is the independence of the change in wind direction. A typical distribution of wind directions in Europe is presented in the following figure. It has to be noted that variation of the wind direction increases especially when a turbine is mounted near buildings. [42]

The main difference of VAWT versus HAWT is related to the nature of the driving torque. When a HAWT is operating in an ideal uniform wind field, the torque produced by each blade is constant independently of the blade angular position. Operation of a H-type rotor is different and much more complicated. The flow geometry varies strongly with the blade angular position. This dependency is illustrated in the flow diagram in Fig. 4 where V_t denotes the tangential velocity of the blade, and V_w represents undisturbed airflow. Therefore, the rotor blades operate in different conditions at every angular configuration.[42]

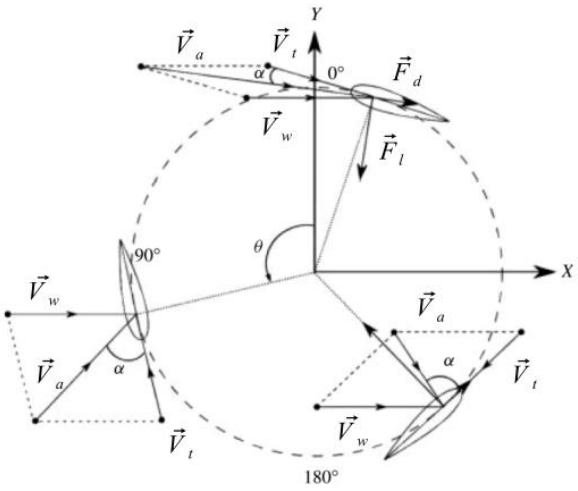

Figure 3.11 Aerodynamics of VAWT [43]

The tangential components of the lift and drag forces produce the shaft torque expressed by [46]:

$$\tau(\theta) = f_L \sin x - f_d \csc x)R,\ \theta\epsilon(0,2\pi)$$

where, R is the rotor radius. Therefore, the H-type rotor is a lift-type wind energy converter. The value of the shaft torque given above is true for every angular configuration. Coefficients C_l and C_d strongly varies with pitch angle and this characteristics is different for every airfoil. This variation is one of the main disadvantages of VAWT. In our discussion NACA 0012H airfoil is considered. Characteristics of many airfoils are widely available in literature. The graph presented in Fig. 4.1 Illustrates dependency C_l and C_d on pitch angle α for the studied airfoil.[24]

To evaluate the pitch angle, the directions of the relative velocity and tangential velocity vectors must be known. The latter vector can be determined from angular position of the blade and its magnitude is $V_t = \omega R$. The value of pitch angle α can be expressed by:

Consequently, the general equations to calculate lift, drag and pitching moment coefficients are as follows:

$$C_D = \frac{F_d}{\frac{1}{2}\rho V^2 A}$$

$$C_L = \frac{F_l}{\frac{1}{2}\rho V^2 A}$$

$$C_m = \frac{M_p}{\frac{1}{2}\rho V^2 AC}$$

Since VAWT does not have to adjust to the wind direction, it does not need a nacelle and a yaw system. Also all heavy components, for example, a generator, may be installed close to the ground. Thus, the overall cost is lower in comparison with HAWT. The biggest disadvantage is its efficiency which is lower than HAWT efficiency. Solutions based on vertical axis wind turbines have about 40% efficiency against 50% efficiency of HAWT.[47]

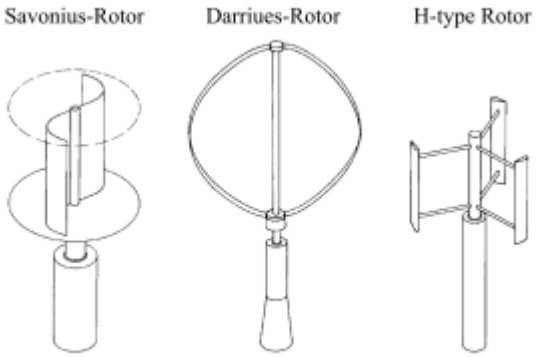

Figure 3.12 Main types of vertical axis wind turbines [46]

H-TYPE ROTOR:

The main aim of this investigation is to increase the efficiency of the H-type rotor. This type of rotor has a few important advantages: the constructional design is relatively simple, blades are usually straight and their cross-section does not change along its axis of rotation. Hence, the computational problem can be reduced to two dimensions. [32] Although the structure of the H-type rotor is simple, the efficiency is still promising and the built cost is one of the lowest in the case of wind turbines. The presented theoretical studies can be verified in a low-cost experiment. The benefits of the proposed solution may be attractive especially for small size customers like individuals, small businesses, and local governments. Therefore, the H-type wind turbines are built mostly on small scale. Here, NACA 0012H airfoil is considered as it is discussed in [23]

Table 4 **NACA 0012h VAWT from Sandia report Reynold's Number = 100,000**

Figure 3.13 : H-type rotor with (NACA012h-sa-50000, rotor diameter 35 m, 300 kW rated power.) [48]

There are 69 values of each parameters in this dataset.[76] Since the pitch angle changes during the rotation of the rotor, the lift force does not reach the maximal possible value for all positions of the blade.

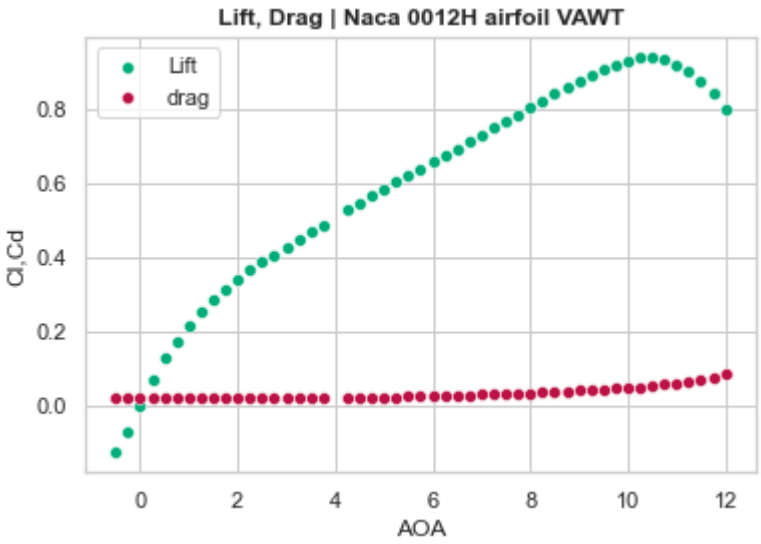

Figure 3.14 Lift, Drag vs. Angle of attack.

Indeed, the best ratio between Cd and Cl occurs when α achieves about 4-6 degrees (for the Reynolds number Re = 50000).

A close observation of L/D curve against **Angle of attack** can find the efficiency of the response (C_l and C_d) variables at the specific angle.

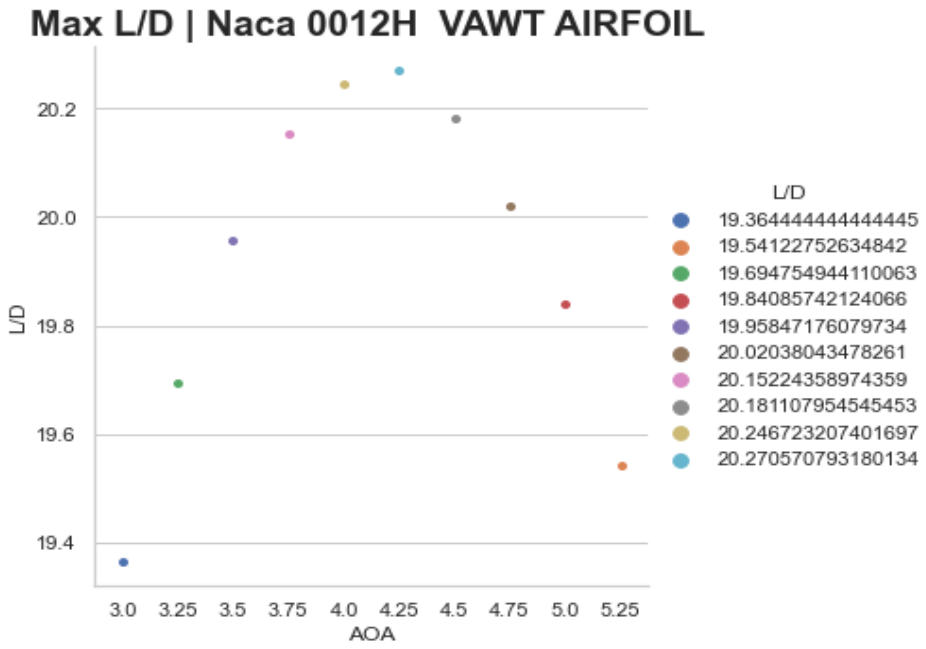

Figure. 3.15 Max. L/D vs. Angle of attack

So, the Maximum L/D is 20. (approximately).In order to maximize the aerodynamically induced torque, an H-type rotor with the AOA control is needed. This solution allows for controlling the value of the AOA to achieve higher values of the lift force (and also higher drag force, unfortunately) in every azimuth position of the rotor.[48].

Perception of Wind energy:

Wind energy is an abundant resource in comparison with other renewable resources. Moreover, unlike the solar energy, the utilization could not be affected by the climate and weather. Wind turbine was invented by engineers in order to extract energy from the wind. Because the energy in the wind is converted to electric energy, the machine is also called wind generator today's rapid increase in energy demands and decaying fossil fuels availability, it is very important to investigate the different alternatives, renewable sources for energy generation. Wind energy is the biggest available source of energy which can easily be harnessed using the mechanical turbines; by converting wind energy into mechanical energy. The energy crisis has become one of the major problems for humanity. With the consumption of fossil fuel and other resources, the world's climate is changing dramatically.[26]

So, environment-friendly energy resources like wind energy have become an auspicious choice for engineers and scientist. Developed countries are now relying more on clean energy than conventional fossil fuels. For instance, in UK, total energy from total wind generation increased by more than one third, offshore wind energy increased by 27 percent (20.9 TWh) [69]. The energy review study by the British Petroleum shows that in 2011, the global primary energy consumption grew by 2.5%; natural gas consumption grew by 2.2%; and oil consumption grew by 0.7%. Coal alone growth by 5.4% and was noted as the fossil fuel to grow above the global average [59]. Coal in 2011 was accounted for 30.3% of global energy consumption and was quoted as having the highest share since 1969 [59]. Considering the environmental consequences of fossil fuel energy systems, the global over dependency on fossil fuels paints a gloomy picture on the earth's environmental system. Further, the over dependency on fossil fuels exerts pressure on the limited energy resources which may seriously affect global economy in the future due to shortage.

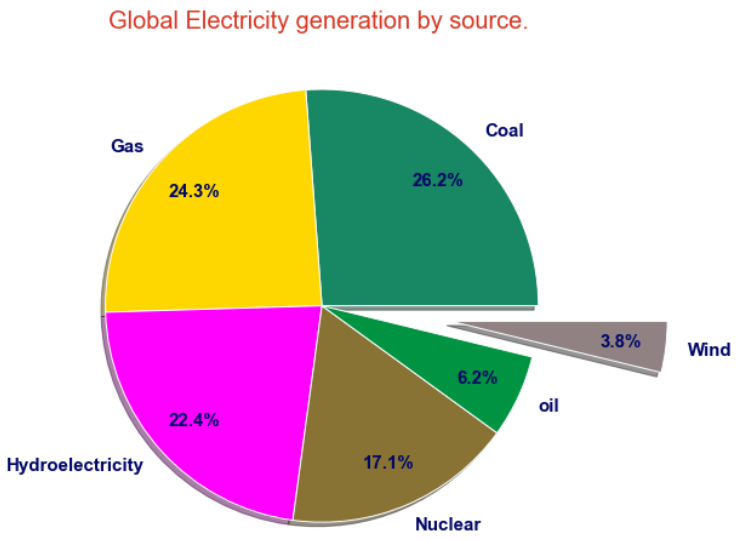

Figure 3.16 Global electricity generation percentage from 2015-2020

Chapter 4

A trade-off study of NACA 2412

What is Trade-off study?

A trade study or trade-off study, also known as a figure of merit empiricism or a factor of merit analysis, is the activity of a multidisciplinary team to determine the most balanced technical solutions among a set of proposed viable solutions.[73]. We want it to generate as much upward force i.e. lift force as possible, without increasing the flow of drag force too much, usually, we aim to establish a balance between lift and drag. As a base design, we select NACA 2412 developed by NACA.

4.1 Inviscid Momentum in Natural Coordinates:

The steady, two-dimensional momentum equations in (*x, y*) coordinates are:

$$\rho\vec{V}.\nabla u = -\frac{\partial P}{\partial x} \qquad (1)$$

$$\rho\vec{V}.\nabla v = -\frac{\partial P}{\partial y} \qquad (2)$$

where $\vec{V} = u\hat{\imath} + v\hat{\jmath}$. Instead of an (*x,y*) coordinate system, these equations can be written in a stream-aligned coordinated system (*r,s*). As shown in Figure 1, *r* is the direction normal to the local streamwise direction and *s* is the local streamwise direction. In this coordinate system, the inviscid momentum equations are:

$$\rho V\frac{\partial V}{\partial s} = -\frac{\partial P}{\partial s} \qquad (3)$$

$$\rho\frac{V^2}{R} = \frac{\partial P}{\partial r} \qquad (4)$$

.

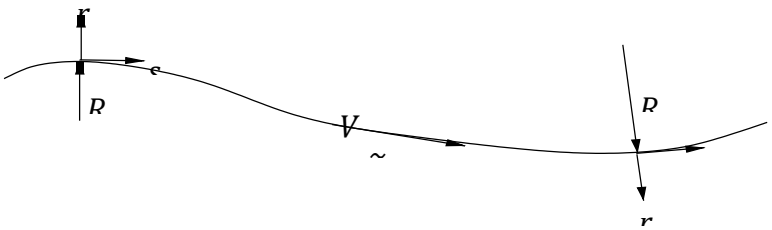

Figure 5.1: Natural coordinate system (*r,s*). *r* is the direction normal to the stream wise direction (along the radius of curvature).

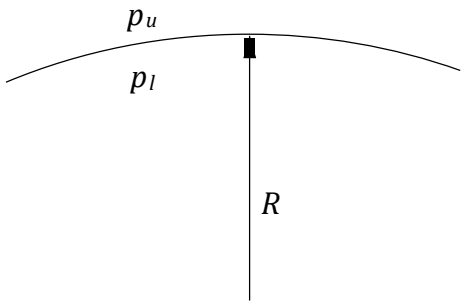

Figure 5.2: Airfoil with a circular shape camber line with radius R and zero thickness. P_u is the upper surface pressure, P_l is the bottom surface pressure.

where $V = |\hat{V}|$ is the magnitude of the velocity vector (i.e. the speed).

For incompressible flow, we note that equation (3) is equivalent to Bernoulli's equation:

$$\rho V \frac{\partial V}{\partial s} = \frac{\partial P}{\partial s} \Rightarrow \quad \frac{\partial}{\partial s}\left(\frac{1}{2}\rho V^2\right) = -\frac{\partial P}{\partial s}$$

$$\Rightarrow \quad \frac{\partial}{\partial s}\left(P + \frac{1}{2}\rho V^2\right) = 0$$

`

$$\Rightarrow \quad P + \frac{1}{2}\rho V^2 = \text{Constant.}$$

4.2 Impact of Camber:

The impact of camber on the pressure distributions can be demonstrated most simply by considering an airfoil with a circular arc camber line and zero thickness as shown in Figure 5.2. Far away from the airfoil, the pressure returns to the free stream pressure P_∞. [31]

On the surface of the airfoil (which must be a streamline), we know that $\partial p/\partial r > 0$ from Equation (4). Thus, above the airfoil, the pressure increases as the distance from the airfoil increases. Since the pressure must eventually return to$p\infty$, this implies that $P_u < P_\infty$. Summarizing the logic chain,

$$\frac{\partial P}{\partial r} = \frac{\rho V^2}{r} > 0$$

$$=> \quad P_\infty - P_u > 0$$

$$=> P_u < P_\infty$$

Similarly, on the lower surface,

$$\frac{\partial P}{\partial r} = \frac{\rho V^2}{r} > 0 \Rightarrow P_l - P_\infty \Rightarrow P_l > P_\infty$$

Combining these results which are based on the curvature of the surface, we see that $P_u < P_\infty < P_l$. Thus, this airfoil will generate lift since the pressure is lower on the upper surface than on the lower surface. Thus, when the maximum camber is at x/c = 0.5, the two circular arcs have the same radius. [32] The C_p distribution for the 0012 at a cl = 0.5 is shown in Figure 3. Recall the definition of C_p is

$$C_p = \frac{P - P_\infty}{1/2\ P_\infty V}$$

Furthermore, the decrease in pressure on the upper surface is nearly equal to the increase in pressure on the lower surface which is reasonable since the radius of curvature is essentially the same on both the upper and lower surface.[35]

4.3 Impact of thickness:

The impact of thickness can also be explained qualitatively from streamline curvature arguments. Consider a symmetric airfoil with thickness. In this case, the curvature of the upper and lower surfaces are in opposite directions. Thus, the logic chain becomes,

$$\frac{\partial P}{\partial r} = \rho\left(\frac{V^2}{R}\right) > 0$$

$$= P\infty - P_u > 0 \Rightarrow\ P_u < P_\infty$$

Similarly, on the lower surface,

$$\frac{\partial P}{\partial r} = \frac{\rho V^2}{R} > 0 \Rightarrow\ P_l - P_\infty < 0 \Rightarrow\ P_l < P_\infty$$

Also, the pressures are lower for the thicker airfoil as would be expected since the radius of curvature is small for the thicker airfoil. On a cambered airfoil, the trends with thickness are similar to the trends on a symmetric airfoil. Specifically, the addition of thickness will tend to lower the C_p on both sizes of the airfoil. [35] Once again, this qualitative behavior can be motivated using streamlined curvature arguments. Increasing the thickness on a cambered airfoil will tend to decrease the radius of curvature of the upper surface, and increase the radius of curvature of the lower surface. Thus, we have the following logic chain, on the upper surface,

$$r \uparrow \quad R \downarrow \quad \frac{\partial P}{\partial r} = \rho \frac{V^2}{R} \uparrow P_\infty - P_u \uparrow \quad P_u \downarrow$$

Similarly, on the lower surface,

$$\mathrm{r} \uparrow \ \mathrm{R} \ \uparrow \frac{\partial \mathrm{p}}{\partial \mathrm{r}} \ = \ \rho \ \frac{\mathrm{V}^2}{\mathrm{R}} \downarrow P_l \ - \ P_\infty \downarrow P_l \downarrow$$

Since the addition of thickness to a cambered airfoil tends to lower both the upper and lower surface pressure and the lift is an integral of the upper and lower surface pressure difference, the resulting lift will be relatively unaffected by thickness. Consequently, thicker airfoils were simulated at the same angles of attack for the corresponding thinner airfoils. For these conditions, the 5 times increase in thickness from 2% to 10% increases the lift by less than 10%. [35]

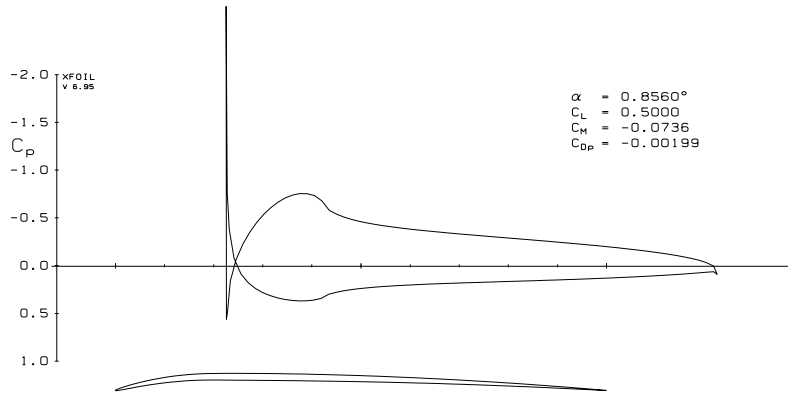

Figure 5.3 NACA 2412, α_∞ = 008560 [31]

4.4 Leading-edge behavior:

We consider the behavior of the flow at the leading edge. As was noted above, the flow will stagnate near the leading edge which results in $C_P = 1$. However, another effect often results in very low pressures at the leading edge. For example, the C_P distribution around the NACA 0012 airfoil at cl = 0.5 shows $C_P < -2$ at the leading edge. The cause of this can be explained also through the streamline curvature argument. In this case, the radius of curvature at the leading edge is very small. And, as $R \rightarrow 0$

$$\frac{\partial \mathrm{p}}{\partial \mathrm{r}} \ = \ \rho \frac{\mathrm{V}^2}{\mathrm{R}} \ \rightarrow \ \infty$$

Thus, the pressures at the leading edge will need to be very low to provide the required force to turn the flow around the leading edge. [31]

Airfoil optimization analysis:

The airfoil optimization process, as shown in fig. 5.4(a) is an iterative process with four discrete steps: updating the airfoil geometry (or starting from an initial design), analyzing the airfoil flow field using CFD analysis, computing the quality of the airfoil by interpreting the flow field, and making changes to the parametric model of the airfoil.[67]

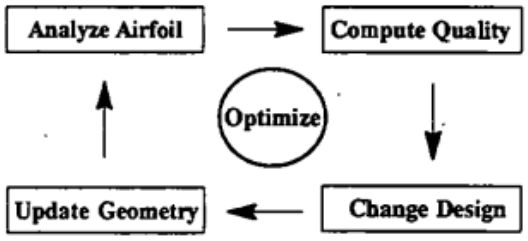

Figure 5.4(a) Quasi-3D section airfoil optimization [67]

Mathematically the problem can be stated as:

$$\text{Max: } F(x), = 1\ldots\ldots n$$

$$\text{s.t. } G(x_i) \leq 0,\ i = 1\ldots..m$$

To formulate airfoil optimization as a standard optimization problem, three primary issues need to be addressed:

- Parametric representation of the design variables.
- evaluation of the CFD solution and
- definitions of the constraint boundaries.[67]

Airfoil choice depends on "best L/D" at a specific but unknown Reynolds number. Typical questions of answers that have been calculated:

i. At which Angle and lift coefficient is the best L/D ratio achieved?
ii. The maximum lift coefficient at the low-speed Reynolds number and higher lift coefficient allows for a smaller wing which produces less friction drag at high speed. The isolated values of best L/D might lead us to a higher drag overall.
iii. What is the behavior of airfoil in a stall? Abrupt lift loss would be a heavy price for a slightly better L/D, so a compromise must be reached.
iv. What is the minimum drag coefficient at low lift coefficients?
v. What is the airfoil thickness in NACA 2412 designs? This determines the structural mass and stiffness of the wing spar. Having a lighter wing might be worth a slightly worse L/D since less lift must be produced.
vi. What is the maximum camber position in NACA 2412 designs? This determines the structural mass and stiffness of the wing spar. Having a lighter wing might be worth a slightly worse L/D since less lift must be produced.[43].

An airfoil is designed to produce lift, but drag is ineluctable. An airfoil that produces the desired lift but causes an excessive amount of drag would not be very useful. We use the lift to drag ratio to determine the efficacy of an airfoil. A high UO ratio indicates a more efficient airfoil. UO is calculated by dividing lift by drag. All terms except C_L and C_D cancel out.[43]

$$\frac{L}{D} = \frac{\frac{1}{2}\,\rho\, V^2\, S\, C_L}{\frac{1}{2}\,\rho\, V^2\, S\, C_D} = \frac{C_L}{C_D}$$

The dataset we use here is a summary of some simulations converged to some final solution, where we test a particular airfoil design (which can vary geometrically)

An aircraft with a width of 2.5% the chord length is placed on a NACA2412 airfoil's upper surface simulating the blowing and suction control at various angle-of-attack. Our NACA 2412 airfoil has Max thickness of 12% at 30% chord and Max camber of 2% at 40% chord. [43]

The current successful large-scale numerical studies create a useful knowledge-based for further exploration of multi-element airfoil design. Summarizing data from our CFD simulations, we will be interested in the parameters that were altered. We'll stick to the lift (upward force) and drag coefficients (resistance force). [63]

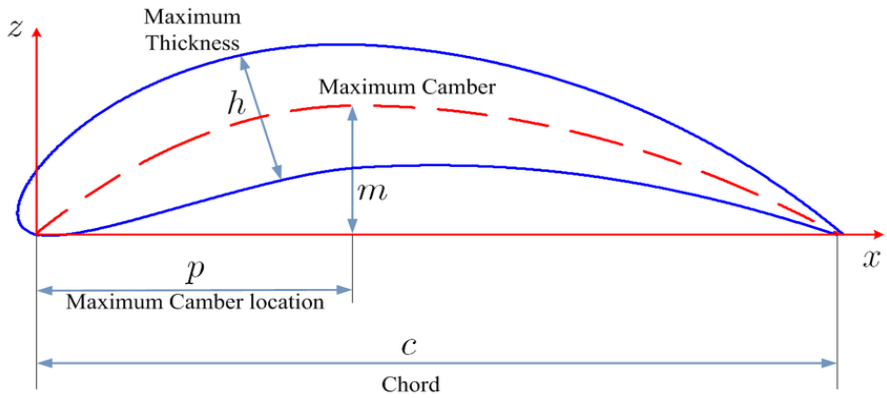

Figure 5.4: A NACA 2412 Cambered Airfoil [43]

The cambered airfoil sections of all NACA families considered herein are obtained by combining a mean line and a thickness distribution. The, necessary geometric data and some theoretical aerodynamic data for the mean lines and thickness distributions may be obtained from the supplementary figures by the methods described for each family of airfoils.[65]

Airfoils can be modified in quite a lot of ways, as designers we need to identify which features of an airfoil to estimate and thus alter.

We will keep things quite elementary & define that will vary in the design of our airfoil:

- The Angle of Attack (AOA)
- Maximum Camber
- Thickness
- Lift-coefficient.
- Drag-coefficient.
- L/D ratio.
- Maximum Camber position.
- Design id

Interpretation of NACA-2412

The NACA 2412 airfoil has a maximum camber of 2% located 40% (0.4 chords) from the leading edge with a maximum thickness of 12% of the chord. The NACA airfoils are airfoil shapes for aircraft wings initiated by the National Advisory Committee for Aeronautics (NACA). [40]The shape of the NACA airfoils is construed by introducing a series of numerals pursuing for the term "NACA". The parameters in the numerical code can be utilized into equations to yield the cross-sectional shape of the airfoil and calculate its following characteristics: [63]

- We will be monitoring the Lift (C_l) & Drag Coefficients (C_d) of the airfoils subsequently will be interested in the ratio of the two (L/D)
- We will be inspecting the results of a design variation study which was conducted using simulations for some of the selected airfoils for NACA 2412 in which we varied some of the parameters shown above, albeit not yet inspected the results of all designs.
- The results need to be analyzed, conclusions about the different designs made, and a subsequent selection of airfoil designs will need to be chosen with a high L/D ratio as potential candidates for the graphical design.

Table 5 Optimization *NACA 2412 (480 design analysis)*

id	design	cd	cl	performance	aoa	maxcamber	maxcamberposition	thickness	L/D
1	Design 1	0.017558	0.815590	-1.012540e-08	5	2.00	40	12.0	46.451719
2	Design 2	0.250152	1.802180	-1.203760e+01	25	7.77	49	25.8	7.204340
3	Design 3	0.135045	-0.315530	-1.003670e+03	-11	6.05	16	8.1	-2.336480
4	Design 4	0.039020	-0.635606	-4.042950e+03	-15	5.18	33	32.9	-16.289236
5	Design 5	0.035562	1.047800	-7.406950e-01	0	9.50	65	22.3	29.464117
...	...	...	...	...	...	...	...	...	...
476	Design 476	0.088358	1.742450	-2.895980e+00	9	9.43	37	1.0	19.720275
477	Design 477	0.141776	2.360070	-5.181080e+00	18	9.01	69	18.4	16.646470
478	Design 478	0.303683	1.110710	-1.593430e+01	17	4.07	46	2.6	3.657465
479	Design 479	0.016545	0.659134	-1.341270e-01	-1	6.58	42	16.3	39.839586
480	Design 480	0.019166	0.974157	1.028260e-01	3	4.91	49	7.3	50.827351

ows × 10 columns

Nearly 500 numerical simulations are conducted over a range of parameters C_l, C_d, angle of Attack, performance, thickness, maximum camber, maximum camber position, which are discussed. L/D has been calculated by diving C_l by C_d

There are 480 designs in this table for NACA 2412. It is hard to exhibit the whole 480 rows of dataset in this paper. ¾ the design parameters are related to the geometry of the airfoil that is (**max camber**, **max camber position** & **thickness**. We plot the relation of the design parameters to the response parameters i.e. lift drag coefficients and L/D. A quick glimpse of the data we are referring to before will be pellucid to comprehend (Table 5). The design name is indicated, as Lift and Drag and the other design parameters or condition parameters.[65]

The dataset we use is a summary of many simulations converged to a final solution, where we test a particular airfoil design NACA 2412 for 480 designs [41] which can vary geometrically. Variation in design can subsequently affect its performance too for example produce upward force.

- The NASA data set comprises different size NACA 2412 airfoils at various wind tunnel speeds and angles of attacks.
- The span of the airfoil and the observer position was the same in all of the experiments. Based on the origin of this dataset it's not certain whether the dataset contains tripped or Non-tripped cases.

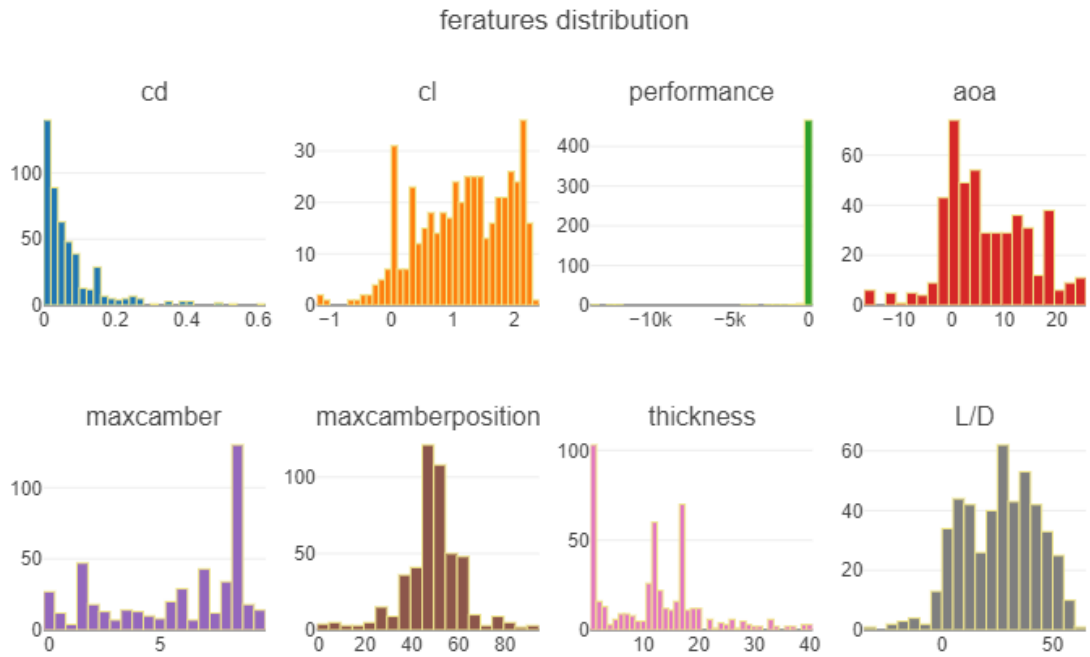

Figure 5.5. A quick visualization of the design data through a Histogram.

In this dataset we let, C_l and C_d are response parameters and all the other are design parameters. **Thickness** has the most nonlinear relation compared to all the other design parameters when it is connected to lift. There tend to be a few values at which lift is maximized. On the other hand variations in drag is quite minimal. As the thickness increases, the lift coefficient C_l deems to decrease gradually.

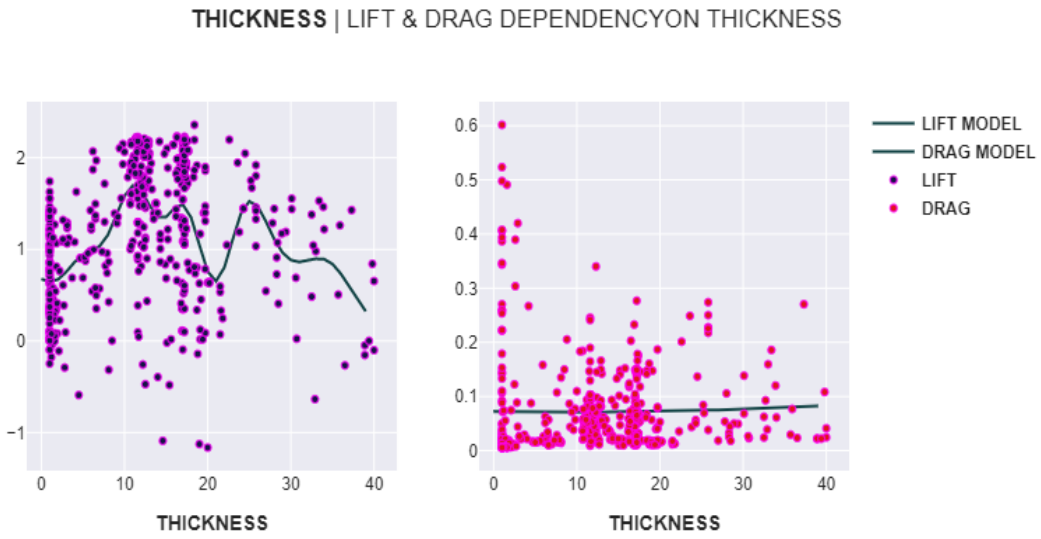

Figure 5.6 Lift, Drag vs. Thickness

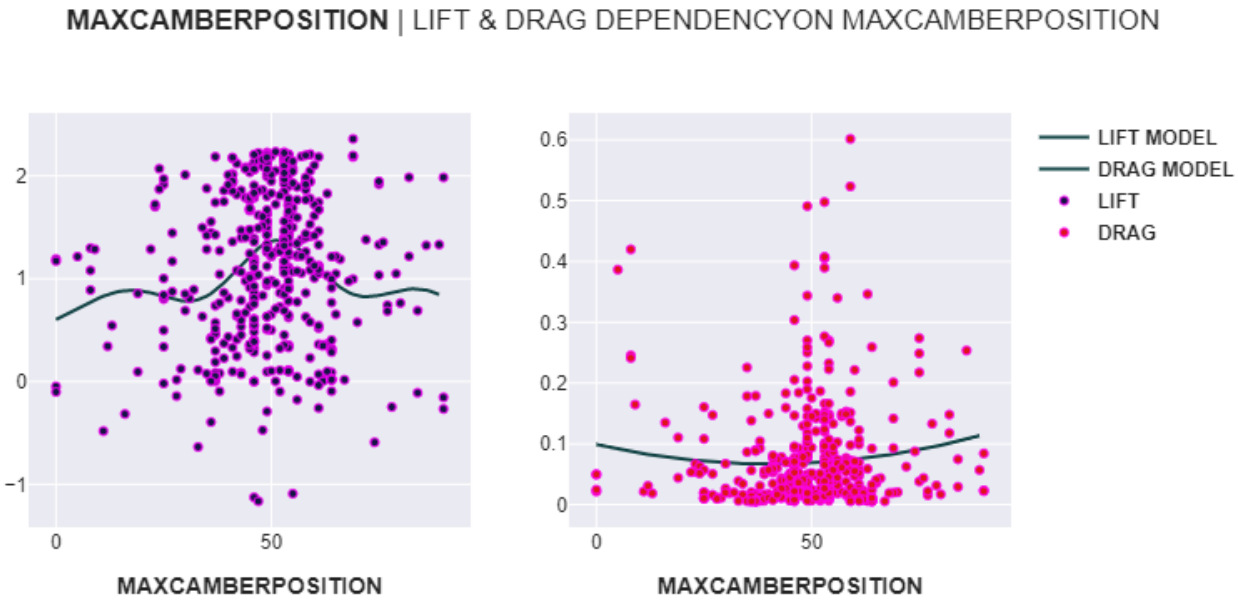

Figure 5.7 Lift, Drag vs. Maximum camber position.

As the **max camber** is increased, the lift generated tends to go up. The drag resistance also tends to go up. **The** relation of **Maximum camber position** to lift is quite nonlinear, we can observe a pinnacle at about the halfway point (50%) on the airfoil, higher and lower values tend to give smaller values of lift. Drag tends to be lower near this point as well. [43]

We want to finish the discussion by having selected a set of designs that would be conducive to the creation of a 3D wing with the aim being. We want it to generate as much upward force as possible, without increasing the flow resistance too much, usually, we aim to strike a balance

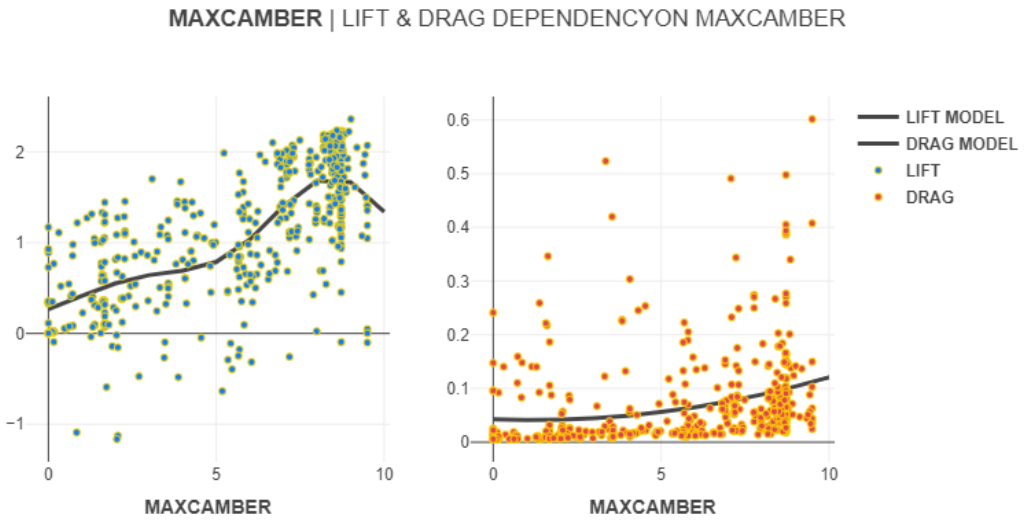

Figure 5.8 Lift, Drag vs. Maximum camber.

Angle of attack parameters:

¼ th of the design parameters & one of the key design parameters is the angle of attack of the airfoil geometry relative to the airflow inflow angle.

Similarly, we create an interpolation model, to exhibit the general trend of all the designs, so we can better understand the relation between lift/drag and the angle of attack.

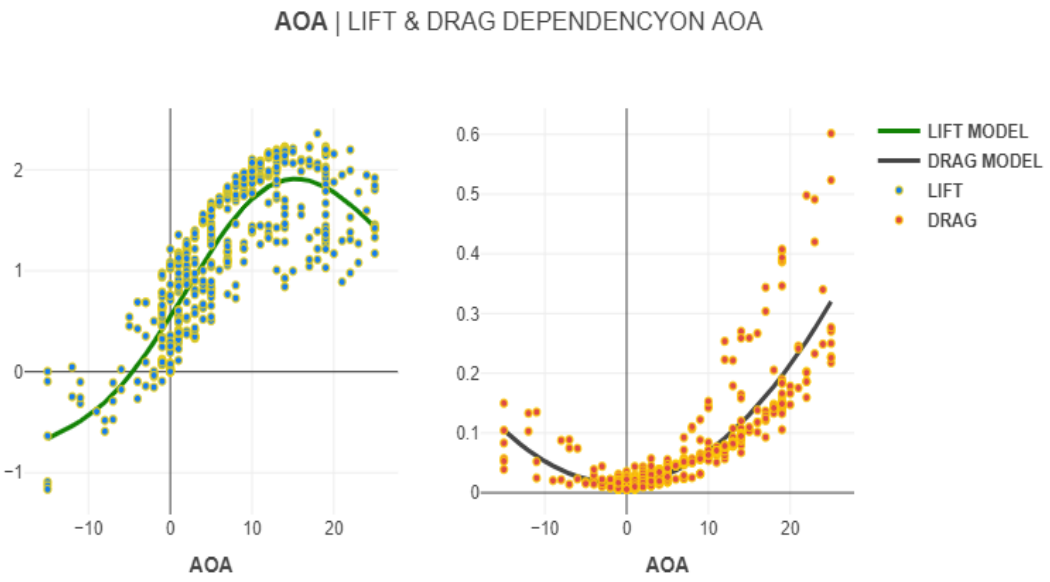

Figure 5.9 Lift, Drag vs. Angle of Attack.

The two models distinctively show what we often see; with the increase in **AOA**, the airfoil starts to generate lift and we have tilted the airfoil enough, we can observe a reduction in the level of production of lift (after a maximum value was reached which is called C_{LMAX} AOA), due to the airfoil is no longer being able to generate any more lift as a result of the exorbitant flow of separation which can consequently result in Stall Phenomenon (sudden loss in altitude). We can predict some designs have very poor lift-producing capabilities as they are below the interpolated model level.

Lift over Drag ratio:

Drag curves are often used to describe the relationship between the lift & drag for any type of lifting device. We can create this addition response variable from the two that we have, C_l & C_d.

We are ferreting for the design that would give us the lowest drag concurrently providing the highest lift possible, consequently, we're focused on the highest lift to drag ratio, i.e L/D ratio [65]. In the figure below for all designs, it is evident that a finite curve begins to emerge abut to the highest gradient i.e. highest L/D ratio. We are looking for designs that would give us the lowest drag whilst providing the highest lift possible, so we're after the highest lift to drag ratio, L/D ratio.

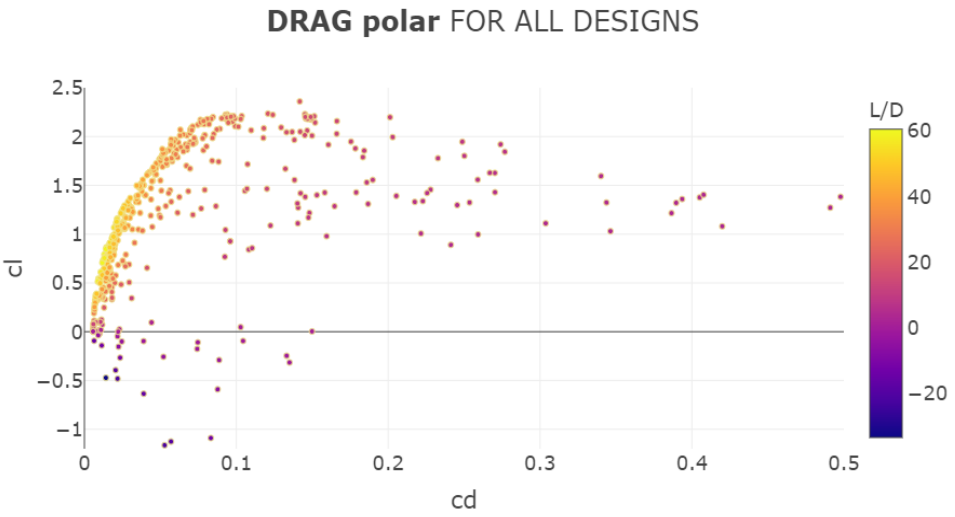

Figure 5.10 DRAG POLAR FOR NACA 2412

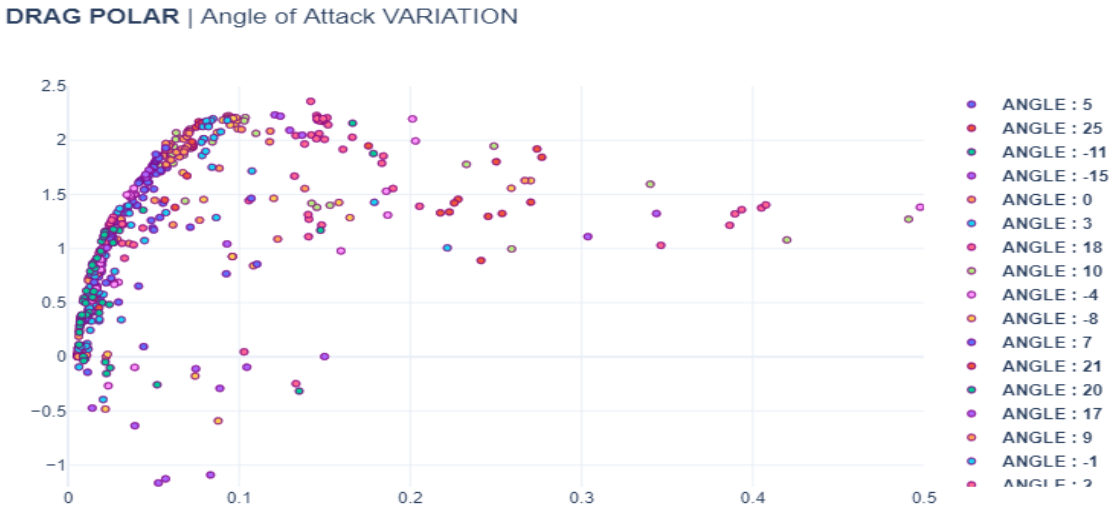

Figure 5.11 DRAG POLAR (Cl vs. Cd) at Angle of attack

Drag polar(Cl/Cd)) over angular subsets:

- We are interested in designs in the vicinity of this high L/D curve. It is indubitable that we have lots of poor designs, implicating in a very high drag value (low L/D).[43]
- Parallel Coordinates are efficient to utilize a legend for all line connections using the C_l and Cd variables, which makes it straightforward to visualize the range of each design required to glean a high L/D ratio. The implementation also allows us to select the desired subset

interactively. The parallel coordinate plot helps us better understand how to design for a high ratio airfoil [44].

- The plot shows all row data (designs) and their resultant value for both parameters (AOA, maximum camber, maximum camber position, thickness) & responses variables (i.e lift/drag coefficients).
- By plotting the designs with a high lift over drag ratio, surely some trends can be seen.

Let us define a modest subset of designs with an L/D ratio of above 55, for instance.

Defining them as a subset with a high L/D aspect to outline some key trends required to acquire high L/D ratio designs.

DESIGN FOR HIGH LIFT/DRAG RATIO:

- We can observe that the drag has to be retained as low as possible whereas generating a little amount of lift (0.51-0.86).
- Rotating the airfoil about (1-3) degrees at maximum, the amount of maximum camber is quite large, which is ideal since we have a significant variety to choose from (3.5-6.7)[63]

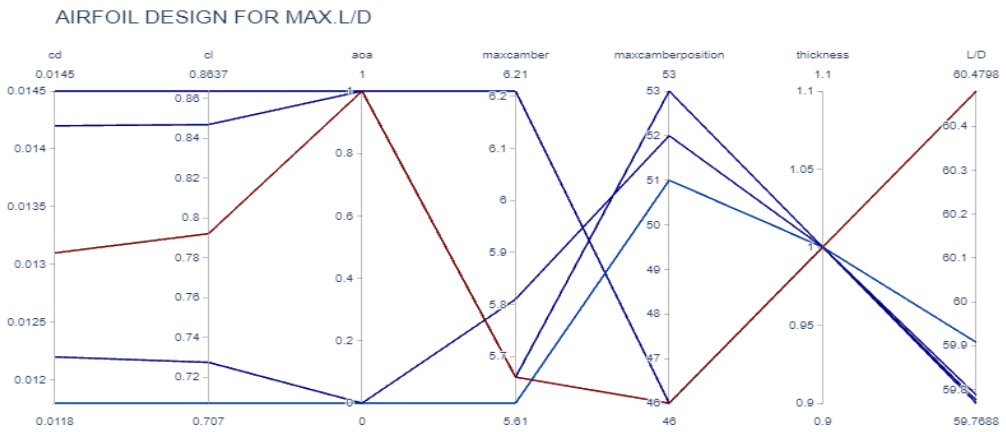

Figure 5.11 Parallel Co-ordinate graph to design for High L/D (Top 5)

- Defining them with a high L/D ratio to outline some key trends are required to obtain high L/D ratio designs. Parallel coordinates are richly interactive by default that drag the lines along the axes to filter regions. The columns are selected to be represented with the design and response parameters i.e. C_l C_d, aoa, thickness, max camber, max camber position etc.[65] Thus, these are the top five designs proposed for obtaining the high L/D ratio concerning aoa, thickness, max camber, max camber position. The top 10 and top 15 designs are exhibited below in the same way.

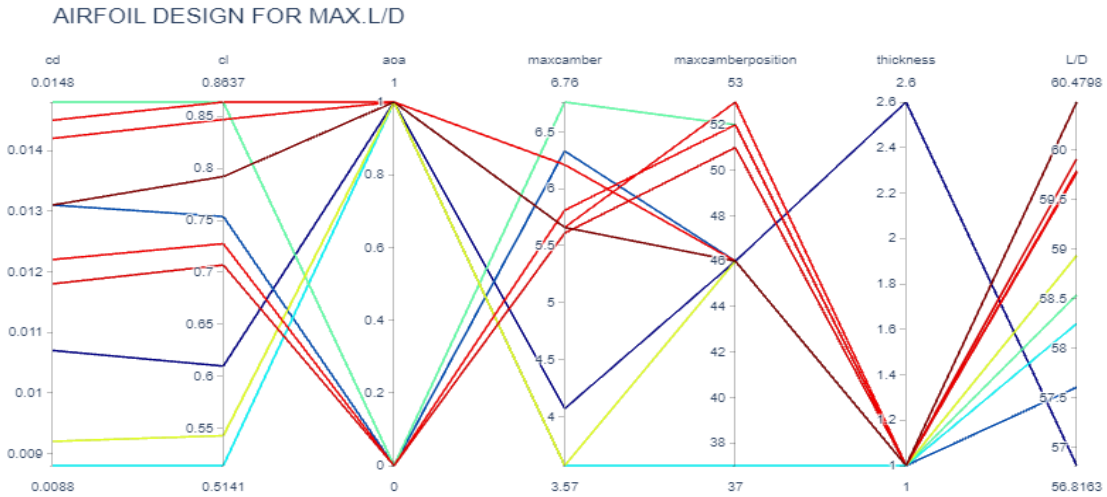

Figure 5.12 Parallel Co-ordinates graph to design for High L/D (Top 10)

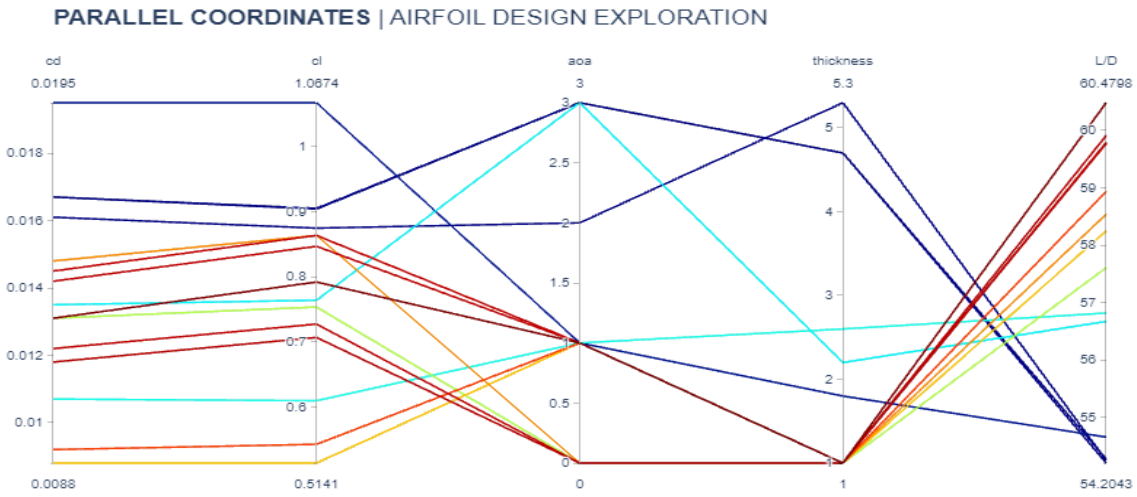

Figure 5.13 Parallel Co-ordinates for High L/D design (Top 15)

Scatter Matrices also exhibit the relation between all variables i.e. **design** and **output variables (i.e. C_l & C_d)** all in one plot as well, which is completely pellucid to comprehend.

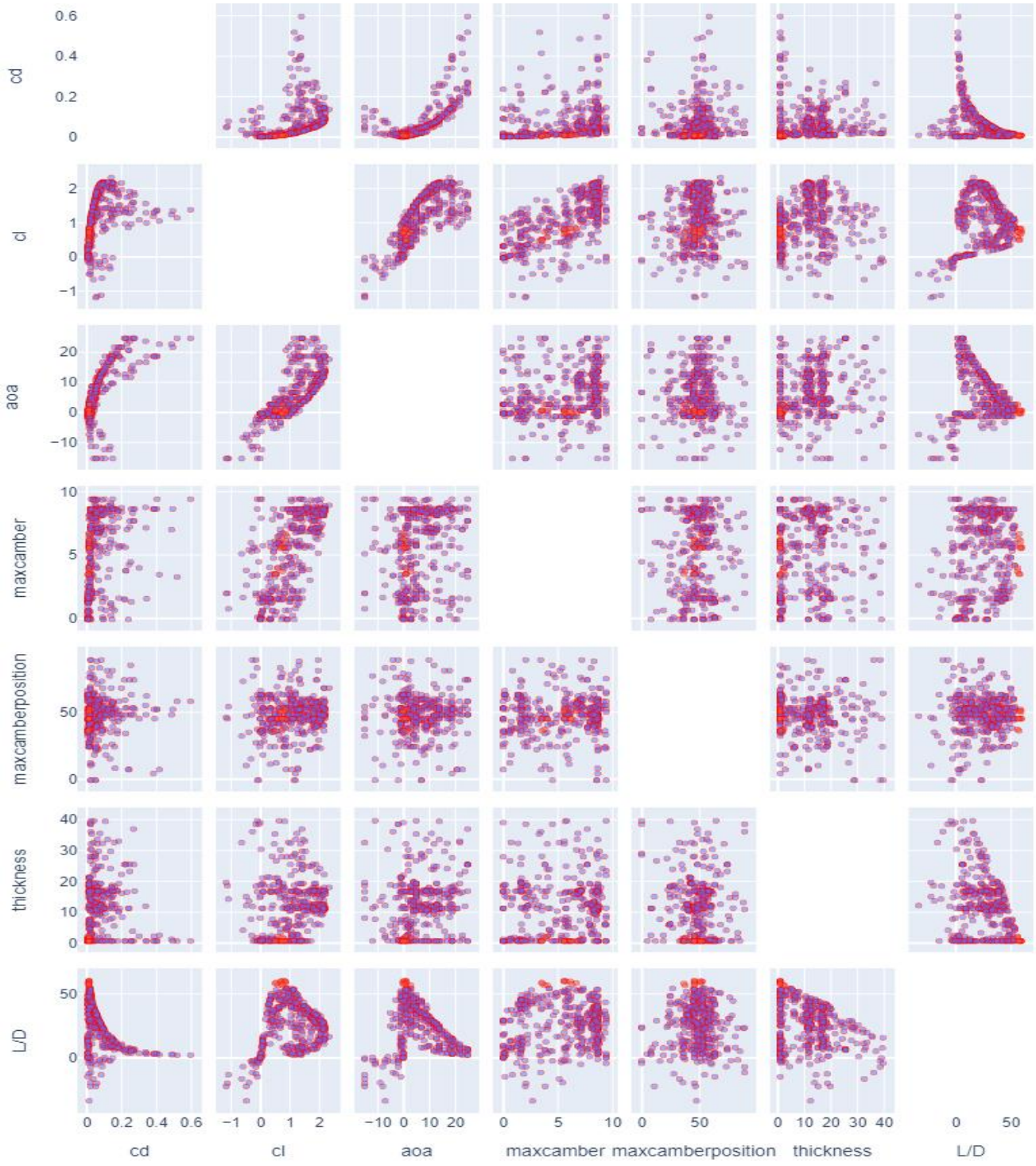

Figure 5.14(c) Scatter Matrix for design exploration.

High L/D analysis:

Table 6 NACA 2412 at Reynold's Number = 50,000:

This dataset has 84 rows and 8 columns. [77]

L/D has been calculated by dividing Cl by Cd.

Mach Number =0

Reynold's number= 50,000

Airfoil name : NACA 2412.

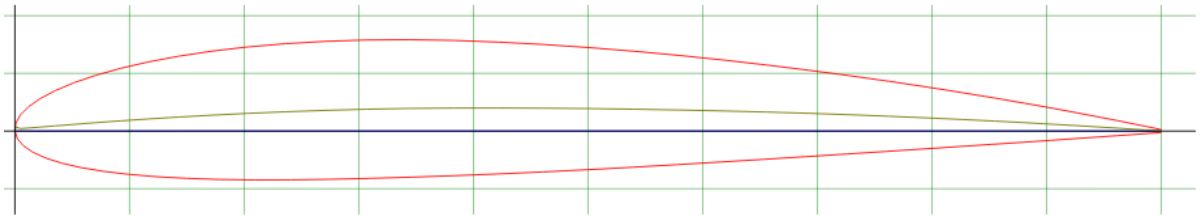

Figure 6. NACA 2412 airfoil [16]

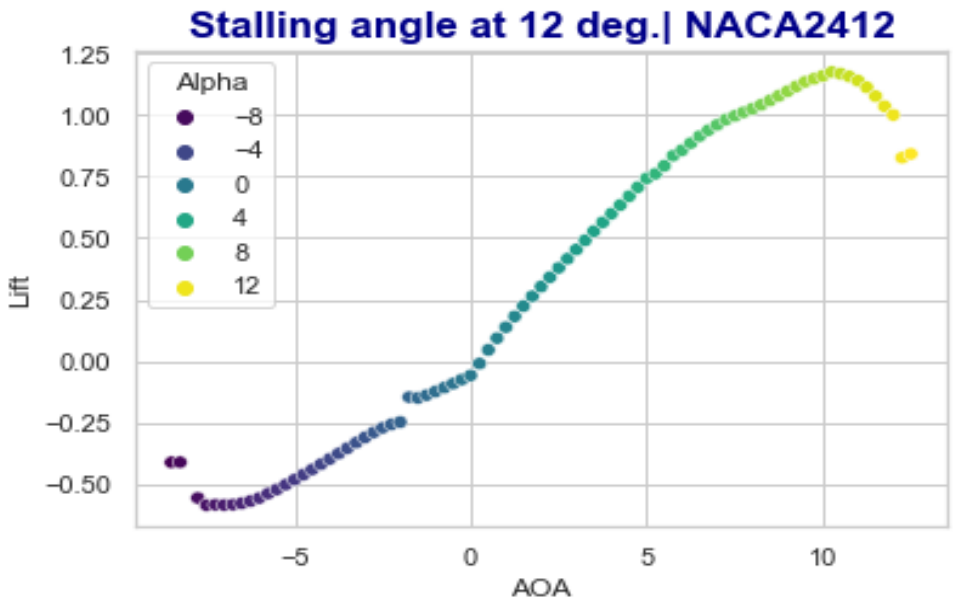

Figure 6.1(a) Lift vs. Angle of attack

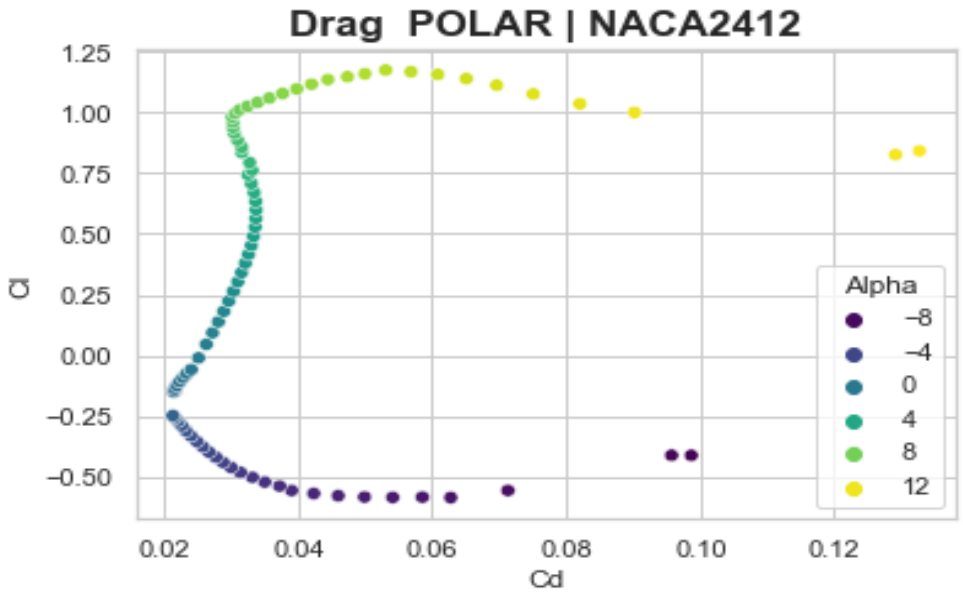

Figure 6.1(b) C_l vs. C_d.

It is evident from **Fig 6.1 (a)** that stall angle is at 11 degrees. Different color of the curve shows the maximum and minimum coefficient of drag and lift and L/D. L/D is maximum approximately at 7-8 degrees. We can observe a close look at this curve

.

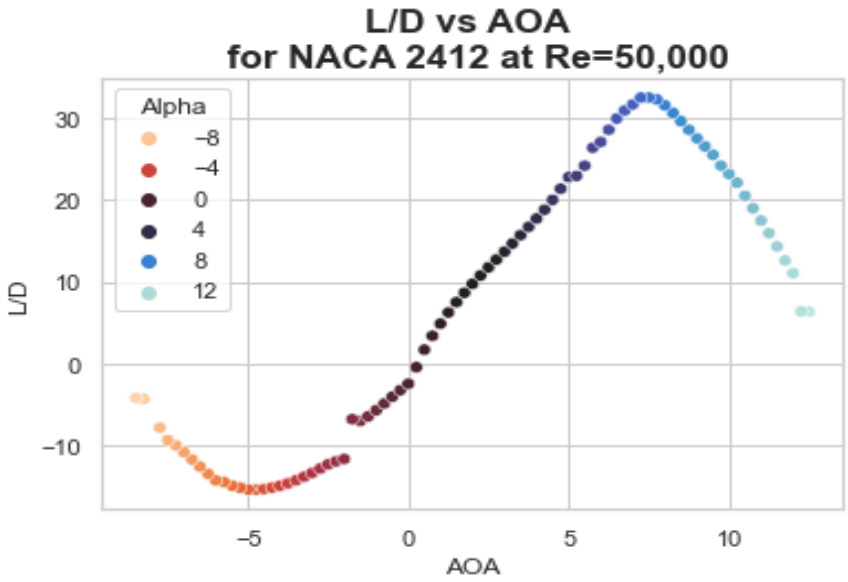

Figure 6.2(a) L/D vs. Angle of attack

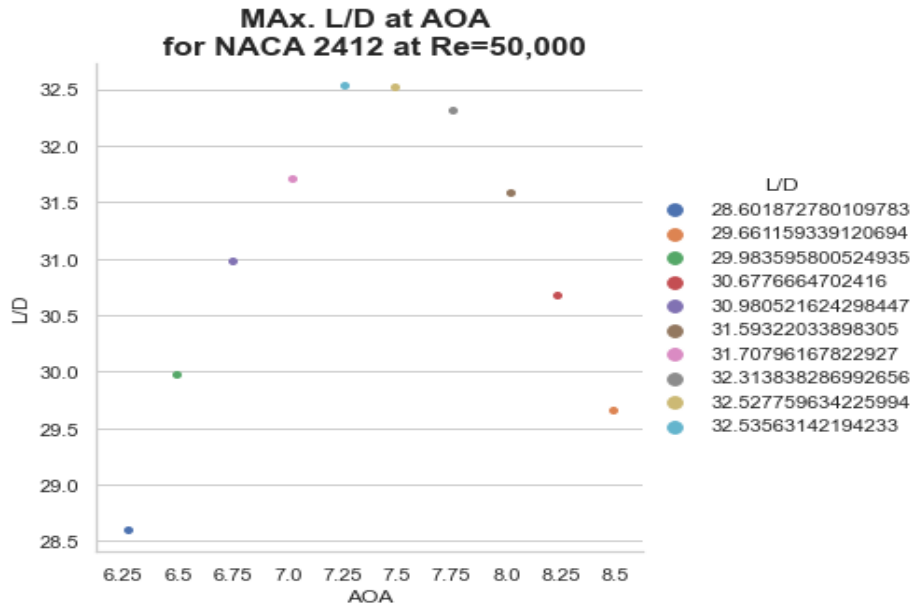

Figure 6.2 (b) Max. L/D vs. Angle of attack

Thus, it is evident that L/D maximum value is 33 (approx.) and most efficient AOA = 7.25-7.5 degrees at Reynold'S NUMBER =50,000.

Comparing NACA 2412 with the symmetric airfoil of **Fig 2.5** where L/D_{MAX}= 27 (approx.) and L/D_{max} aoa = 5.5 degrees. Clearly NACA 2412 produces high lift than symmetric airfoil NACA 0012.

Table 7 **NACA 2412 at Reynold's Number=100,000:**

The following data is for NACA 2412 at Reynold's Number=100,000 [79]

Reynolds number fixed and Mach number =0 (fixed).

There are 112 rows of parameters in this dataset. [80] . L/D has been calculated for by C_l/C_d.

It is evident that stalling angle is at 15 degrees and the best ratio between Cd and Cl occurs when α achieves about 5-10 degrees for, NACA 2412 the Reynolds number Re = 100,000.

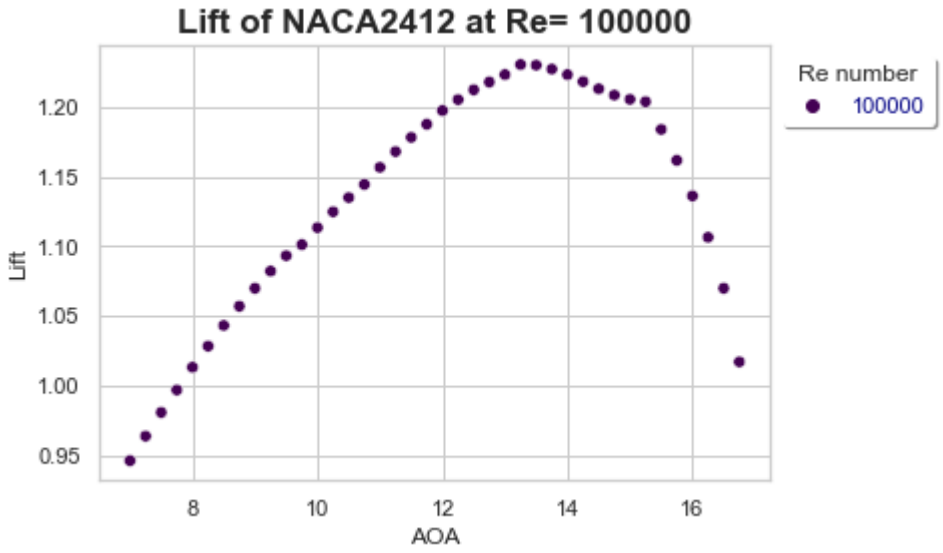

Figure 6.3 Lift vs Angle of attack.

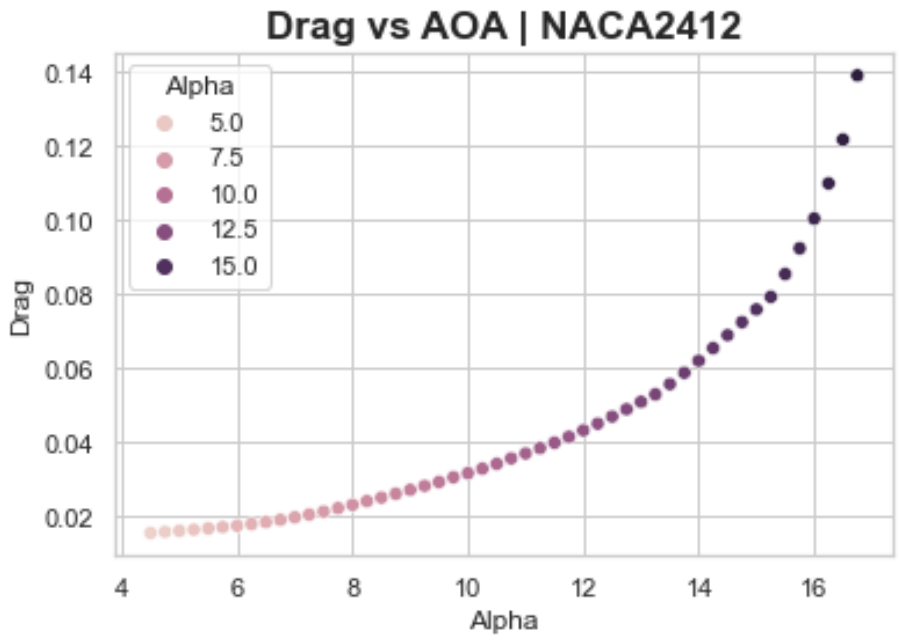

Figure 6.4 Drag vs Angle of attack.

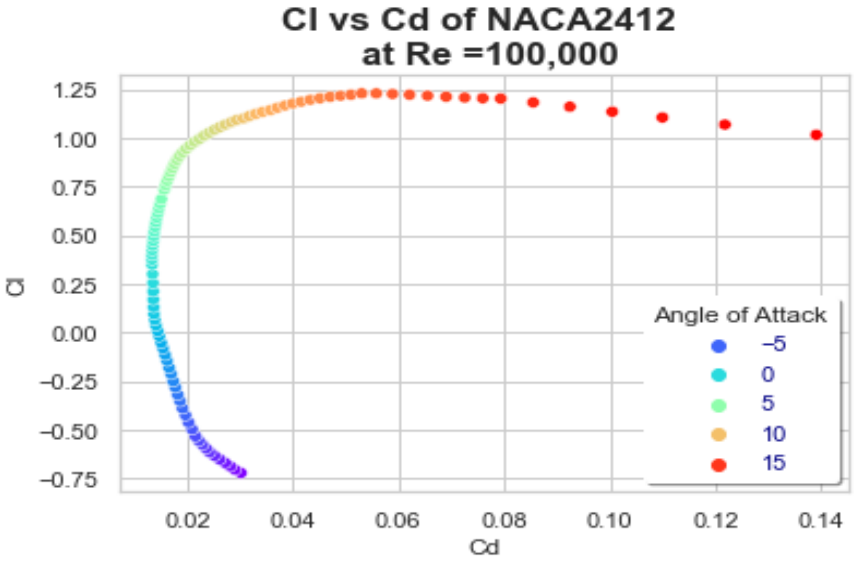

Figure 6.5 C_l vs. C_d

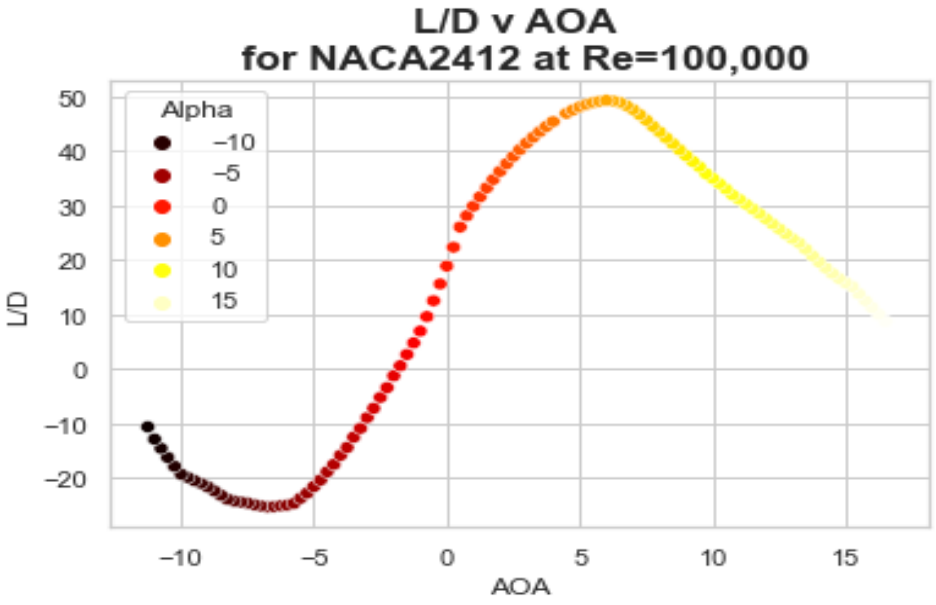

Figure 6.6 L/D vs. Angle of attack

A close look at this curve in Fig 6.5 shows that The L/D is 49.35(approx.) at R_e = 100,000 and the efficient AOA is at 6^0 in this airspeed.

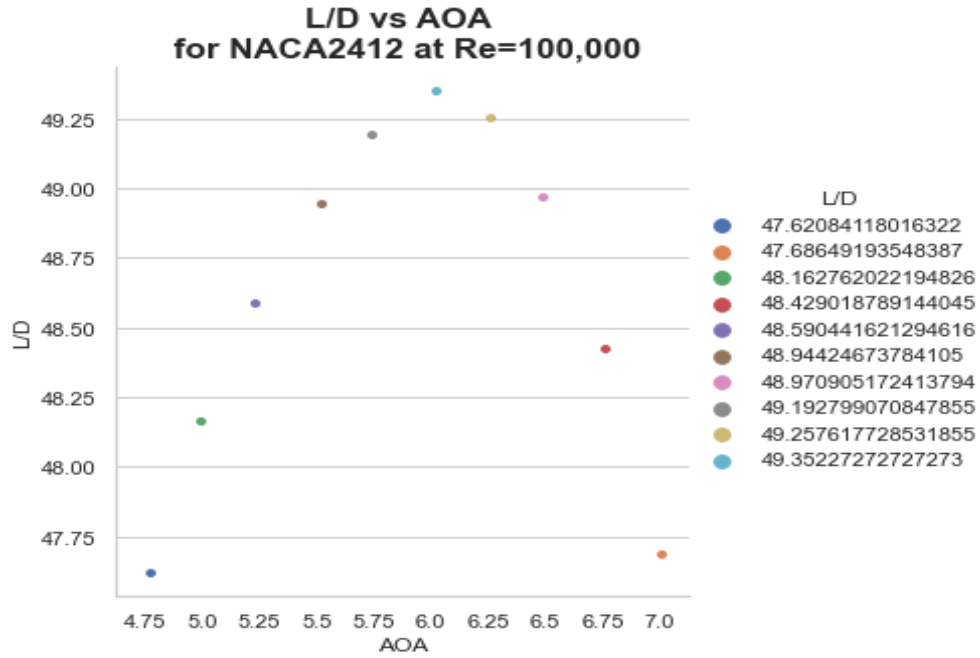

Figure 6.7 Max. L/D on specific angle of attack

Similarly for Reynold's number= 200,000, the Lift and drag varies in higher angle of attack comparing with lower airspeed. As the flow tends to be more turbulent, the L/D ratio also tends to maximize at a lower angle of attack. It is found that stalling occurs at 16 degrees at R_e = 200,000 and the best ratio between C_d and C_l occurs when α achieves about 5-6 degrees for NACA 2412. A close look at this curve shows that The L/D is 87.5 at R_e = 200,000 and And the efficient AOA is at 5^0 in this airspeed. Thus, at different wind speed the airfoil has different L/D.

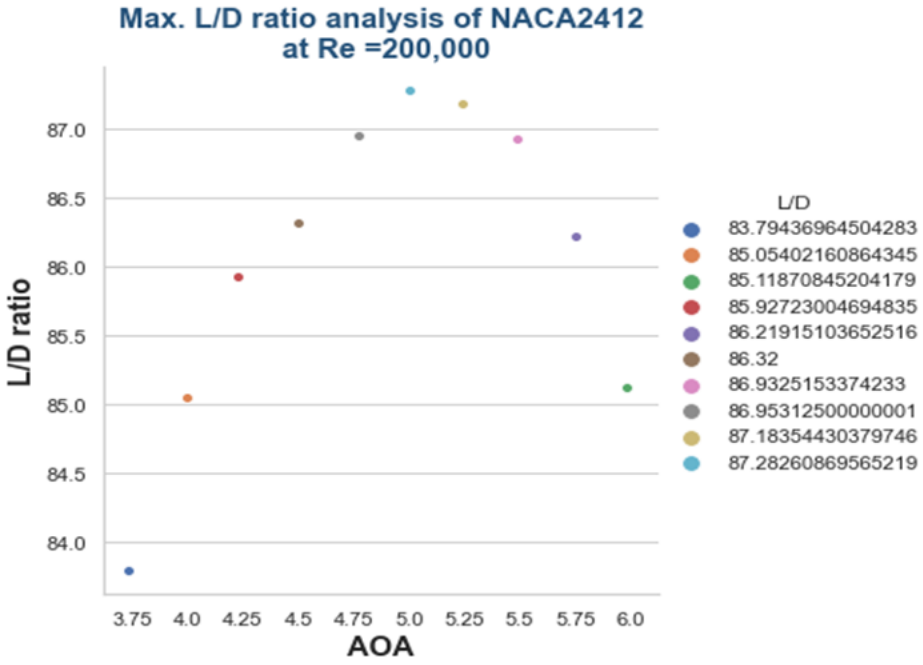

Figure 6.8 Max. L/D on specific angle of attack.

It is evident that higher airspeed creates higher L/D ratio at lower Angle of attack. The more the airflow is turbulent, the more L/D ratio is produced by NACA 2412. Combining the above tables for NACA 2412 and calculating L/D, the **efficiency** of NACA 2412 in different wind speed has been visualized.

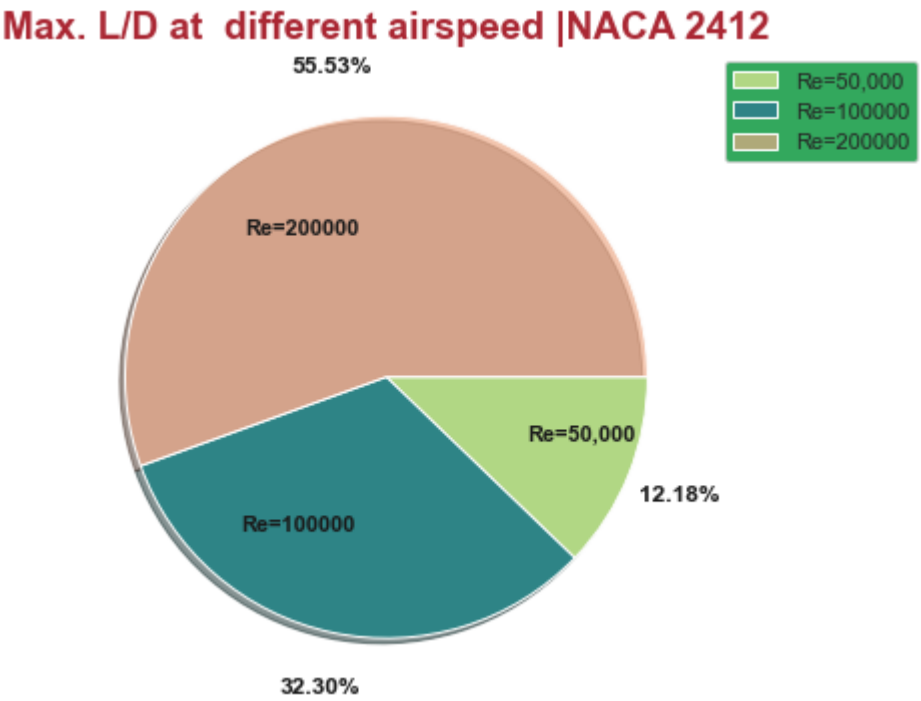

Figure 6.9 Efficiency of NACA 2412 at different airspeed.

Figure 6.10 Aircraft Raytheon T400 use NACA 2412 [41]

Comparing NACA 2412 with NACA 2415

Table 8 NACA 2415 at Reynold's Number = 100,000

The dataset has 110 rows and 7 columns [81].

L/D has been calculated by dividing Cl by Cd.

Mach Number =0

Reynold's number= 100,000

Airfoil name : NACA 2415

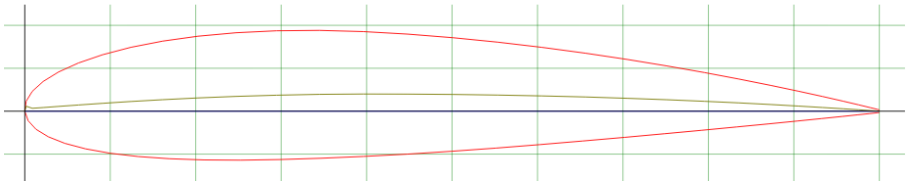

Figure 6.11 NACA 2415 [11]

Figure 6.12: NACA 2415 and 2412 airfoils are used in Cessna 172.[66]

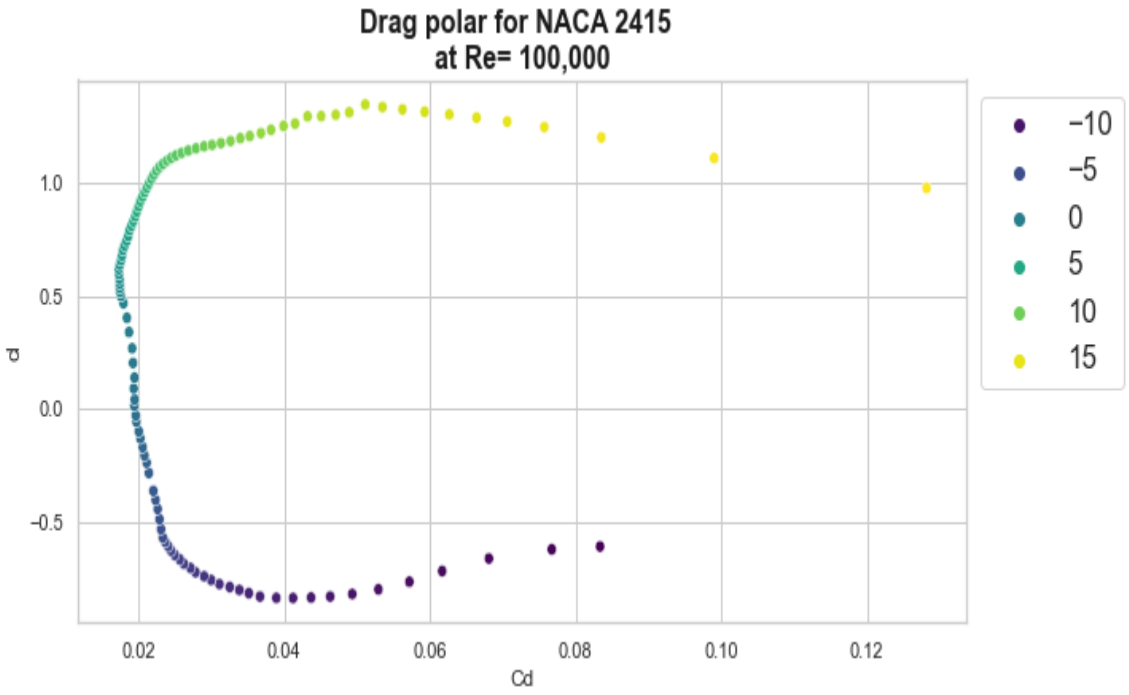

Figure 6.13 C_l vs. C_d

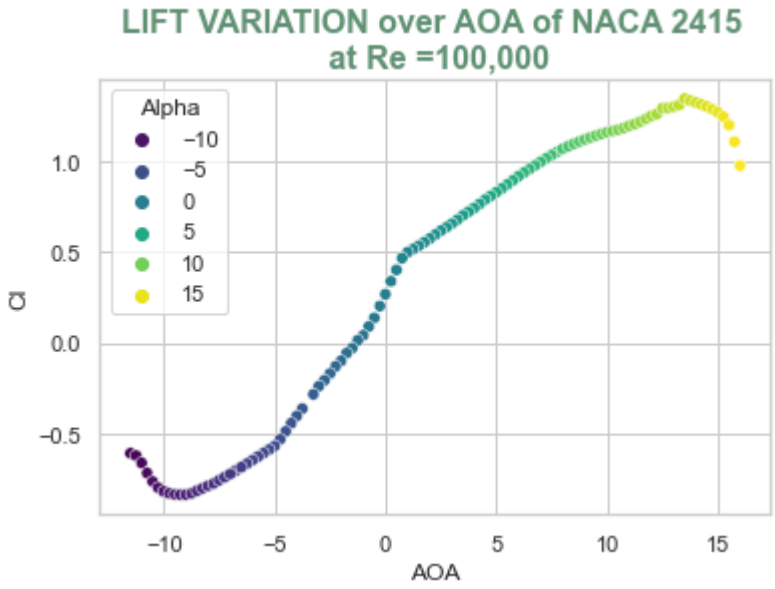

Figure 6.13 Lift vs. AOA

The stalling for this airfoil occurs at around 14 degrees which causes a sudden decrease in altitude. Drag is minimum from 0-5 degrees.

Fig 6.15 shows that L/D is maximum at the angle of attack 7.5 degrees at Re = 100,000Thus, we need to keep the AOA below 5 degrees to keep the pitch moment as minimum as well as lift maximum.

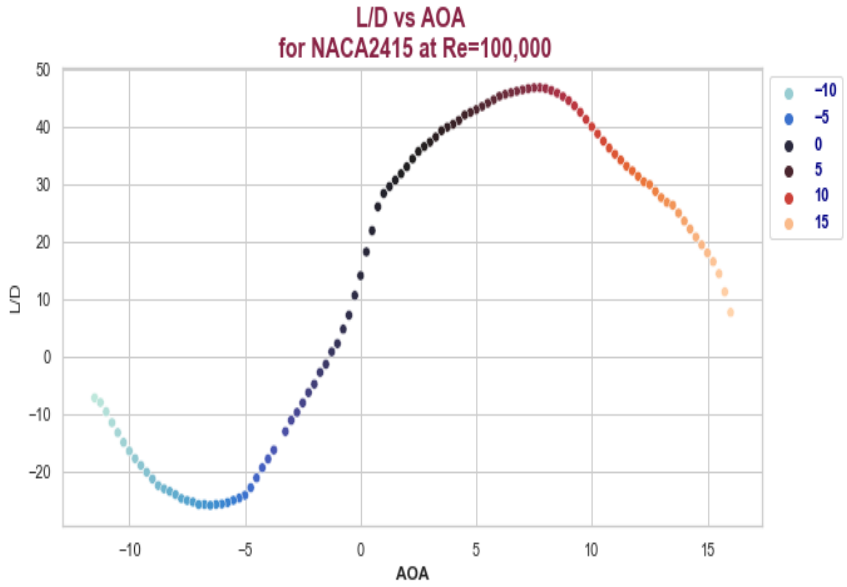

Figure 6.14 L/D vs. AOA

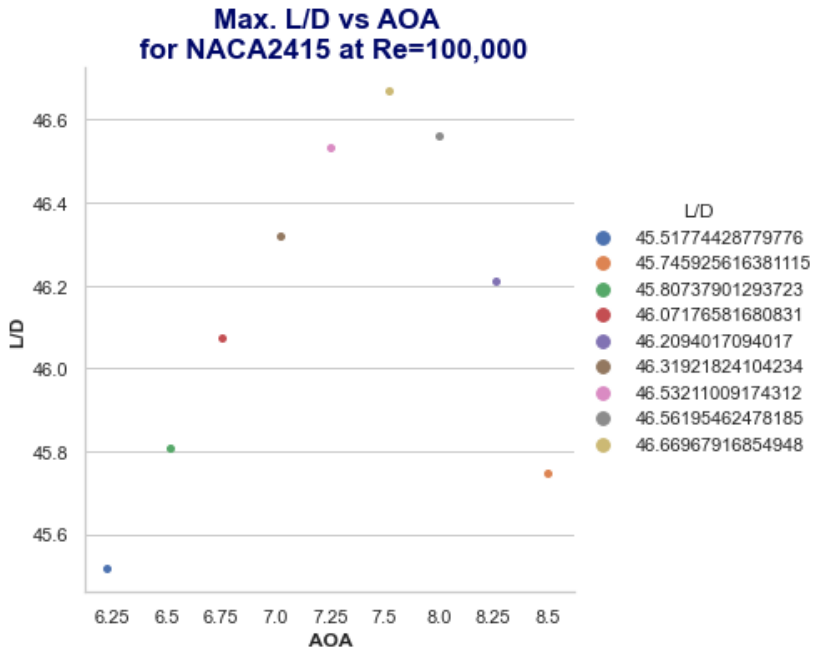

Figure 6.15 Max. L/D on specific angle of attack

The most efficient AOA or C_{LMAX} AOA is 7.5 for max. L/D which is 47(73pprox..

- Thus, at low wind speed, NACA 2412 airfoil is more efficient (50 at a lower angle of attack) in maximizing L/D reconciling with NACA 2415 which is 46.67 at 7.5 degree AOA.

Chapter 5

Results and Discussions:

After testing several designs of the airfoil NACA 2412 through some step analysis, the results show which steps should be applied for high lift. We looked at the design variable (input parameters) i.e. thickness, angle of attack, maximum camber, , maximum camber position in relation to response variables (Lift and drag) & defined an additional response from the two existing, L/D. Even with four sets of input parameters of Table-2, the range of variation in both C_l & C_d was quite large.

Having created a model for the design variable in relation to both lift and drag variables, we saw a significant deflection from this value, indicating a very broad range of available designs. Shifting our focus on obtaining the highest L/D ratio, we were able to note that a large number of high L/D cases were associated with midrange lift values in NACA 0012, NACA 2412, NACA 2415, at different Reynold's number also keeping the drag to a minimum. We should curb the angle of attack as small as possible (0^0-5^0 degrees).

Higher Reynold's number produces more efficiency of airfoils and stall at higher Angle of Attack, thus high L/D ratio. Cambered airfoils produce a greater L/D ratio than symmetric airfoils e.g. NACA 0012. In our NACA 2412 optimization design, the addition of camber is very conducive.(1/5 % - 9.5%) .The maximum camber position needs to be in the core part of the airfoil (between 25% and 75%).The thickness of the airfoil should be at the slightest. (1% to 12%) in NACA 2412. Shifting our focus on obtaining the highest L/D ratio, we were able to note that a large number of high L/D cases were associated with mid-range lift values, thus keeping the drag to a minimum. It is mandatory to keep the angle of attack as low as possible, this provides a wide advantage for the variables associated with desired L/D ratio.A particular aircraft's required lift is set by its C_l/C_d, delivering that lift with lower drag results directly in better fuel economy in aircraft, climb performance, and glide ratio. The Parallel Coordinate plots were very useful in the visualization of multi feature relations, specially, when related to our desired variable, L/D. Consequently, a model for L/D was created using all the available design variables as the feature matrix.

In HAWT, The pitch angle for blades should be between 7 degrees to 10 degrees for better structural performance as L/D is maximum at this range. In wind turbines, a solution with a variable pitch angle is promising to indicate an increase in the turbine efficiency by 22.6%. The considerations have a preliminary nature, and they correspond just to a fragment of the computational studies.

The best L/D ratio of several airfoils along with NACA 2412 have been calculated and visualized with several scatterplots to find out the most efficient angle of attack which can significantly reduce fuel consumption of aircrafts during take-offs and lifting at any stage of \\the flight. Addition of High lift devices such as flaps and slats of various types can reduce further fuel consumption in such airfoils during take-offs and landing.

References

1. Winslow, J., Otsuka, H., Govindarajan, B., & Chopra, I. (2018) Basic understanding of airfoil characteristics at low Reynolds numbers (104–105). *Journal of Aircraft*, *55*(3), 1050–1061. https://doi.org/10.2514/1.C03441
2. Collis SS, Joslin RD, Seifert A, Theofilis V. Issues in active flow control: theory, control, simulation, and experiment. Progress in aerospace sciences. 2004 May 1;40(4-5):237-89.
3. Aziz MA, Islam MS. Effect of Lower Surface Modification On Aerodynamic Characteristics of an Airfoil. InInternational Conference on Mechanical Engineering and Renewable Energy 2017.
4. Anderson JD. Inventing Flight: the Wright brothers & their predecessors. JHU Press; 2004.
5. Lindhe Norberg UM. Structure, form, and function of flight in engineering and the living world. Journal of morphology. 2002 Apr;252(1):52-81.
6. Cherne J, Culick F, Zell P. The AIAA 1903 Wright'Flyer'Project Prior to Full-Scale Tests at NASA Ames Research Center. In38th Aerospace Sciences Meeting and Exhibit 2000 Jan 10 (p. 511).
7. Blackwell TJ. Subsonic Wind-Tunnel Wall Corrections On A Wing With A Clark Y-14 Airfoil. A Masters Project Presented to The Faculty of the Department of Mechanical and Aerospace Engineering San Jose State University. 2011 May.
8. Raymer, D. P. "Aircraft Design: A Conceptual Approach". S.L.: AIAA Educational Series, 2002.
9. Kroo, I. and Shevell, R., "Aircraft Design: Synthesis and Analysis," Digital Textbook, Desktop Aeronautics, Stanford, CA, 2001.
10. Selig MS, Guglielmo JJ. High-lift low Reynolds number airfoil design. Journal of aircraft. 1997 Jan;34(1):72-9. Sripawadkul, Vis & Padulo, Mattia & Guenov, Marin. (2010). A Comparison of Airfoil Shape Parameterization Techniques for Early Design Optimization. 10.2514/6.2010-9050.
11. I. Paraschivoiu, NASA. Lewis Research Center, Wind Turbine Dynamics 19–25 (1981).
12. Jacobs, Eastman N. (National Advisory Committee for Aeronautics). NASA Technical Reports Server [Internet]. 1939 [Updated: 1996]. Available from: https://ntrs.nasa.gov/search.jsp?R=1993009278
13. Shevell RS. Fundamentals of flight. Pearson Education India; 1989.
14. An Experimental Study on the Aerodynamic Performance of Winglets with Curve Edged Wing of NACA 4412 By Ismat Ara.
15. Radespiel R, Heinze W. SFB 880: fundamentals of high lift for future commercial aircraft. CEAS Aeronautical Journal. 2014 Sep 1;5(3):239-51.
16. Narramore JC, Olander RD, Stearman RO. The Development of a Computer Aided Airfoil Design Procedure Including Preliminary Wind Tunnel Experiments on a Low Reynolds Number High Lift Section. Volume I. TEXAS UNIV AT AUSTIN AUSTIN; 1976 Jan 1.
17. An Experimental Study on the Aerodynamic Performance of Winglets with Curve Edged Wing of NACA 4412 By Ismat Ara.
18. Whitcomb, Richard T.: Review of NASA Supercritical Airfoils. ICAS Paper No. 74-10, Aug. 1974.

19. Data-based Approach for Fast Airfoil Analysis and Optimization Jichao Li Mohamed A. Bouhlel Joaquim R. R. A. Martins

20. ESDU 84026. Aerofoil Maximum Lift Coefficient for Mach Numbers up to 0.4. Engineering Science Data Unit, 1999.
21. Pfeiffer NJ. Slotted airfoil with control surface. In2018 Applied Aerodynamics Conference 2018 (p. 3958).
22. Computer Program To Obtain Ordinates for NACA Airfoils Charles L. Ladson, Cuyler W. Brooks, Jr., and Acquilla S. Hill Langley Research Center, Hampton, Virginia Darrell W. Sproles Computer Sciences Corporation Hampton, Virginia
23. Shevell RS. Fundamentals of flight. Pearson Education India; 1989.
24. Oler, J. W., et al. *Dynamic-stall regulation of the Darrieus turbine*. No. SAND-83-7029. Texas Tech Univ., Lubbock (USA). Dept. of Mechanical Engineering, 1983
25. Design of a new urban wind turbine airfoil using a pressure-load inverse method J.C.C. Henriques a, F. Marques da Silva b , A.I. Estanqueiro c , L.M.C. Gato
26. Tangler, J., et a1., "SERI Advanced Wind Turbine Blades," International Solar Energy Society.
27. Tangler, J., et ai, "Measured Structural Loads for the Micon 65/13, "ASMEIETCE Wind Energy Symposium," New Orleans, Louisiana, January, 1994.
28. Gai, S. L., and Palfrey, R., "Influence of Trailing-Edge Flow Control on Airfoil Performance," Journal of Aircraft, Vol. 40, No. 2, 2003, pp. 332-337.
29. Aerodynamic Measurement System. For Unmanned Aerial Vehicle Airfoils. JOURNAL OF SYSTEMICS, CYBERNETICS AND INFORMATICS.
30. Lift Generation and Streamline Curvature Prof. David L. Darmofal Department of Aeronautics and Astronautics Massachusetts Institute of Technology.

31. Caygill P. Sound Barrier: The Rocky Road to MACH 1.0+. Pen and Sword; 2006 Oct 30.
32. DESIGN OF AN AERODYNAMIC MEASUREMENT SYSTEM FOR UNMANNED AERIAL VEHICLE AIRFOILS L. Velázquez-Araque1 and J. Nožička1 1 Department of Fluid Dynamics and Power Engineering, Faculty of Mechanical Engineering Czech Technical University in Prague, Czech Republic.

33. Mueller-Vahl H, Strangfeld C, Nayeri CN, Paschereit CO, Greenblatt D. Thick Airfoil Deep Dynamic Stall. InWind Energy-Impact of Turbulence 2014 (pp. 35-40). Springer, Berlin, Heidelberg.

34. Bousman WG. A qualitative examination of dynamic stall from flight test data. Journal of the American Helicopter Society. 1998 Oct 1;43(4):279-95.
35. Mary I, Sagaut P. Large eddy simulation of flow around an airfoil near stall. AIAA journal. 2002 Jun;40(6):1139-45.
36. Rudolph PK. High-lift systems on commercial subsonic airliners.

37. Storms, B. and Ross, J., "Experimental Study of Lift-Enhancement Tabs on a Two Element Airfoil," Journal of Aircraft, Vol. 32, 1995, pp. 1072-1078.
38. Lee, H. T., Kroo, I. M., and Bieniawski, S., "Flutter Suppression for High Aspect Ratio Flexible Wings Using Microflaps," AIAA Paper 2002-1717, Denver, CO; 22-25 Apr. 2002.

39. Stanewsky, E., "Adaptive Wing and Flow Control Technology," Progress in Aerospace 37, 2001, pp. 583-667. [13] D.P. Jansen, Passive Flow Separation Control on an Airfoil-Flap ModelThe Effect of Cylinders and Vortex Generators. Delft University of Technology, August 2012.
40. The NACA airfoil series.doc (stanford.edu).
41. Sóbester, András, and Tom Barrett. "Quest for a Truly Parsimonious Airfoil Parameterization Scheme." *The 26th Congress of ICAS and 8th AIAA ATIO*. 2008.

42. C. Lin. Control of turbulent boundary-layer separation using micro-vortex generators. AIAA Journal, 3404:99, 1999.

43. Jakubowski, Mateusz & Starosta, Roman & Fritzkowski, Pawel. (2018). Kinematics of a vertical axis wind turbine with a variable pitch angle. AIP Conference Proceedings. 1922. 110012. 10.1063/1.5019115

44. Caygill P. Sound Barrier: The Rocky Road to MACH 1.0+. Pen and Sword; 2006 Oct 30.

45. Dey S, Saha R. CFD study on aerodynamic effects of NACA 2412 airfoil as rear wing on a sports car. no. December: 0–6. 2018 Dec.
46. Wing and Airfoil Optimized Design of Transport Aircraft J Allan Antunes Lyrio Technological Institute of Aeronautics (ITA).
47. R. E. Sheldahl and P. C. Klimas, Aerodynamic Characteristics of Seven Symmetrical Airfoil Sections Through 180-Degree Angle of Attack for Use in Aerodynamic Analysis of Vertical Axis Wind Turbines (National Technical Information Service, Springfield, 1981)
48. Airfoil Boundary Layer Optimization Toward Aerodynamic Efficiency of Wind Turbines Youjin Kim, Ali Al-Abadi and Antonio Delgado Additional information is available at the end of the chapter http://dx.doi.org/10.5772/
49. Dynamic Stall Investigation of Two-Dimensional Vertical Axis Wind Turbine Blades Using Computational Fluid Dynamics Mahdi Hasan1,a), Asif Kabir2, b) and Yeasir Mohammad Akib.
50. WIND ENERGY EXPLAINED Theory, Design and Application Second Edition J. F. Manwell and J. G. McGowan Department of Mechanical and Industrial Engineering, University of Massachusetts, USA A. L. Rogers DNV – Global Energy Concepts, Washington, USA.
51. Storms, B.L.; Jang, C.S. (1994). "Lift Enhancement of an Airfoil Using a Gurney Flap and Vortex Generators". Journal of Aircraft 31 (3): 542–547. doi:10.2514/3.46528.
52. R. E. Sheldahl and P. C. Klimas, Aerodynamic Characteristics of Seven Symmetrical Airfoil Sections Through 180-Degree Angle of Attack for Use in Aerodynamic Analysis of Vertical Axis Wind Turbines (National Technical Information Service, Springfield, 1981).
53. Our world in data.org/power generation.
54. "FLUID STRUCTURE INTERACTION OF WIND TURBINE BLADE USING COMPUTATIONAL FLUID DYNAMICS.

55. L.M.M. Boermans and P.B. Rutten. Two-dimensional aerodynamic characteristics of airfoil NLF-MOD22with fowler flap. Technical report, TU Delft, 1995.
56. NREL's S809 Airfoil - NREL HAWT airfoil S809 primary 21.0% Re=2.0E+6 Clmax(S)=1.00 Restrained max lift coefficient.
57. Stivers LS, Abbott IH, von Doenhoff AE. Summary of Airfoil Data. 1945 Mar.

58. Storms BL, Jang CS. Lift enhancement of an airfoil using a Gurney flap and vortex generators. Journal of Aircraft. 1994 May;31(3):542-7..

59. Wickens, R. H. Wind Tunnel Investigation of Dynamic Stall of an NACA 0018 Airfoil Oscillating in Pitch (Etude en Soufflerie du Decrochage Aerodynamique d'un Profil NACA 0018 Oscillant en
60. Tangage). NATIONAL AERONAUTICAL ESTABLISHMENT OTTAWA (ONTARIO), 1985.

61. Kaunda CS, Kimambo CZ, Nielsen TK. Hydropower in the context of sustainable energy supply: a review of technologies and challenges. International Scholarly Research Notices. 2012;2012.

62. Nelson RC. Flight stability and automatic control. New York: WCB/McGraw Hill; 1998 Mar.

63. Whitcomb, R. T., "A Design Approach and Selected Wind-Tunnel Result at High Subsonic Speed for Wing Tip Mounted Winglets", NASA TN D-8260, 1976.
64. Oler, J. W., et al. *Dynamic-stall regulation of the Darrieus turbine*. No. SAND-83-7029. Texas Tech Univ., Lubbock (USA). Dept. of Mechanical Engineering, 1983.

65. Aerodynamics of a NACA2412 Airfoil in Ground Effect M. R. Ahmed The University of the South Pacific, Suva, Fiji and T. Takasaki† and Y. Kohama Tohoku University, Sendai 980-8577, Japan. DOI: 10.2514/1.238752.

66. Sunanda A, Nayak MS. Analysis of NACA 2412 for automobile rear spoiler using composite material. International Journal of Emerging Technology and Advanced Engineering. 2013 Jan;3(1):230-8.
67. Aerodynamic Analysis of Multi Element Airfoil D.Vimal Chand, R.Sriram, D.Udaya Kumar U.G Student, Dept. of Aeronautical, Jeppiaar Engineering College,Chennai,India.
68. TURBINE AIRFOIL DESIGN OPTIMIZATION Sanjay Goel General Electric Company Corporate Research and Development Schenectady, New York John I. Cofer IV Hardev Singh General Electric Company Industrial and Power Systems Schenectady, New York.
69. UK ENERGY IN BRIEF 2018, Department of Business, Energy & Industrial Strategy, 1 Victoria Street, London SW1H 0ET

70. Nabhan MB, Seddiq EK. Study in Reduction of Vortex Drag at Low Cruising Aircraft Speeds. Journal of Advance Research in Mechanical & Civil Engineering (ISSN: 2208-2379). 2018 Oct 31;5(10):01-19.

71. Gamboa P, Vale J, Lau FJ, Suleman A. Optimization of a morphing wing based on coupled aerodynamic and structural constraints. AIAA journal. 2009 Sep; 47(9):2087-104.

72. Sun, Junzi & Hoekstra, Jacco & Ellerbroek, Joost. (2020). Estimating aircraft drag polar using open flight surveillance data and a stochastic total energy model. Transportation Research Part C: Emerging Technologies. 114. 391-404. 10.1016/j.trc.2020.01.026.

73. https://en.wikipedia.org/wiki/Trade_study

74. Voona R. Enhancing the aerodynamic performance of stepped airfoils.
75. http://airfoiltools.com/polar/csv?polar=xf-n0012-il-50000-n
76. NACA0012H for VAWT from Sandia report SAND80-2114, http://airfoiltools.com/airfoil/details?airfoil=naca0012h-sa (), accessed: 2017-07-30

77. http://airfoiltools.com/polar/csv?polar=xf-n2412-il-50000-n
78. NRELS809HAWT from Sandia report SAND80-2114,http://airfoiltools.com/polar/csv?polar=xf-s809-il-50000-n
79. http://airfoiltools.com/polar/csv?polar=xf-n2412-il-100000-n

80. http://airfoiltools.com/polar/csv?polar=xf-n2415-il-100000-n

81. http://airfoiltools.com/polar/csv?polar=xf-n2412 optimization-n